Fault damage zone volume and initial salinity distribution determine intensity of shallow aquifer salinization in geological underground utilization

E. Tillner[1], M. Langer[1], T. Kempka[1] and M. Kühn[1,2]

[1]{GFZ German Research Centre for Geosciences, Telegrafenberg, 14473 Potsdam, Germany}

[2]{University of Potsdam, Institute of Earth- and Environmental Science, Karl-Liebknecht-Str. 24/25, 14476 Potsdam, Germany}

Correspondence to: E. Tillner (elena.tillner@gfz-potsdam.de)

Abstract

Injection of fluids into deep saline aquifers causes a pore pressure increase in the storage formation, and thus displacement of resident brines. Via hydraulically conductive faults, brine may migrate upwards into shallower aquifers, and lead to unwanted salinization of potable groundwater resources. In the present study, we investigated different scenarios for a potential storage site in the Northeast German Basin using a 3D regional scale model that includes four major fault zones. The focus was on assessing the impact of fault length and the effect of a secondary reservoir above the storage formation, as well as model boundary conditions and initial salinity distribution on the potential salinization of shallow groundwater resources. We employed numerical simulations of brine injection as a representative fluid using the simulator TOUGH2-MP.

Our simulation results demonstrate that the lateral model boundary settings and the effective fault damage zone volume have the greatest influence on pressure build-up and development within the reservoir, and thus intensity and duration of fluid flow through the faults. Higher vertical pressure gradients for short fault segments or a small effective fault damage zone result in the highest salinization potential due to a larger vertical fault height affected by fluid displacement. Consequently, it has a strong impact on the degree of shallow aquifer salinization, if a gradient in salinity exists or the salt-freshwater interface lies below the fluid

displacement depth in the faults. A small effective fault damage zone volume or low fault permeability further extend the duration of fluid flow, which can persist for several tens to hundreds of years, if the reservoir is confined laterally. Laterally open reservoir boundaries, large effective fault damage zone volumes and intermediate reservoirs significantly reduce vertical brine migration and the potential of freshwater salinization because the origin depth of displaced brine is located only a few decametres below the shallow aquifer in maximum.

The present study demonstrates that the existence of hydraulically conductive faults is not necessarily an exclusion criterion for potential injection sites, because salinization of shallower aquifers strongly depends on initial salinity distribution, location of hydraulically conductive faults and their effective damage zone volume as well as geological boundary conditions.

1 Introduction

Carbon Capture and Storage (CCS) can contribute to the reduction of global anthropogenic carbon dioxide emissions. Different geological underground formations have been suggested as target storage sites, such as deep saltwater-bearing aquifers (saline aquifers) providing the worldwide largest storage potential as part of the earth's widely distributed sedimentary basins (IPCC, 2005). Shallow aquifers in sedimentary basins can comprise considerable freshwater resources, which in turn are of great importance for regional water supply. However, brine displacement due to the elevated pore pressure in the storage formation is one potential risk of CO_2 storage in deep saline aquifers. Saline fluids could reach shallower freshwater aquifers through different migration pathways, and significantly impair groundwater quality. Especially fault zones are of particular importance, as they might transect several caprocks and thus can provide large-scale permeable conduits between aquifers at different depths (Dempsey et al., 2014; Fitts and Peters, 2013; Chiaramonte et al., 2008; IEAGHG, 2008; Bense and Person, 2006; Forster and Evans, 1991).

Displacement of brine and potential freshwater salinization as a result of CO_2 storage has been investigated in several studies. Table 1 summarizes the initial conditions and essential results of numerical simulations concerning this issue. The models applied are either synthetic (Birkholzer et al., 2011; Oldenburg and Rinaldi, 2011; Birkholzer et al., 2009) or refer to a certain study area (Tillner et al., 2013; Zouh et al., 2010; Yamamoto et al., 2009; Nicot, 2008). Several studies examine pressure perturbation and resulting brine migration in a

multi-barrier system without considering vertical conduits. It was shown that pressure build-up can be observed in a distance of more than 100 km from the injection zone (Birkholzer et al., 2009). The choice of boundary conditions and petrophysical parameters have a crucial impact on the pressure development, as demonstrated by two independent studies considering industrial-scale CO_2 injection in the Illinois Basin (Person et al., 2010; Zhou et al., 2010). After Person et al. (2010), the pressure perturbation is limited to a distance of about 25 km from the injection location for a total injection rate of 80 Mt CO_2 $year^{-1}$, whereas Zhou et al. (2010) simulated a pressure build-up as far as 300 km from the injection area (100 Mt CO_2 $year^{-1}$). The disparity between the simulation results is mainly related to the fact that Person et al. (2010) assumed considerably lower reservoir formation permeability, higher formation compressibility and closed lateral flow boundaries except for the northern model domain, whereas Zhou et al. (2010) applied laterally open flow boundaries (Table 1).

However, upward brine migration only occurs if pressure perturbation in the reservoir is large enough to overcome the weight of the fluid column in a vertical conduit. If a steady-state is reached or continuous flow develops further depends on the magnitude of pressure increase, and whether brine is allowed to spread unhindered in the upper aquifer due to a continuous hydraulic connection throughout the formation without barriers to flow (Birkholzer et al., 2011; Oldenburg und Rinaldi, 2011). As stated previously, especially faults can represent vertical conduits, which may have an essential influence on groundwater flow and brine migration due to their extent and distribution in the Earth's upper crust. Nevertheless, a meaningful implementation of complex geological structures into a sufficiently discretised model grid is very difficult, especially at regional scale. Tillner et al. (2013) investigated the influence of permeable faults on brine displacement referring to a real study area. The authors simulated upward brine migration through complex fault systems depending on reservoir compartmentalisation and fault permeability, whereby faults were implemented by the virtual element approach (Nakaten et al., 2013). The results of Tillner et al. (2013) show that the degree of pressurization is the driving mechanism for brine migration, while an increase of fault permeability from 100 mD by two orders of magnitude had no significant impact on the salinization of shallower aquifers. Their investigations focused on the prospective storage site Beeskow-Birkholz (in the following only referred to as Beeskow) in Northeast Germany, which is also considered in this work.

Here, we present a regional scale 3D model with a simplified geometry, neglecting topographic variations of the formation tops and bases while the four considered fault zones are implemented with their complex arrangement and curvature to focus the analysis on clearly identifiable effects of fault fluid flow. The presumed simplifications further significantly improved the convergence efficiency of the simulations and avoided numerical artefacts. In different leakage scenarios the impact of fault lengths, hydrogeological boundary conditions, initial salinity distribution and the presence of an overlying secondary reservoir on upward brine displacement were assessed to deepen our understanding on potential freshwater salinization resulting from geological CO_2 storage in deep saline formations.

2 Study area

The potential CO_2 storage site is located close to the town Beeskow in the Northeast German Basin (NEGB; Fig. 1a). In a respective industrial project and according to the estimated storage capacity, it was planned to inject 34 Mt CO_2 over a period of 20 years (1.7 Mt CO_2 $year^{-1}$) into the basal sandstones of the Detfurth Formation from the Middle Buntsandstein (Lower Triassic); (Vattenfall, 2009, 2010). Porous and fractured sediments of the lower Muschelkalk (Middle Triassic) represent a secondary suitable reservoir above the target storage horizon (Fig. 2a). A multi-barrier system of different caprocks, mainly anhydrites, halites and claystones from the Upper Buntsandstein, the Middle and Upper Muschelkalk, as well as the Lower Keuper seals the Detfurth Formation and the overlying secondary reservoirs. The basal sandstones of the Rupelian (Oligocene, Upper Tertiary) at a depth between 100 m and 150 m in average mark the beginning of saltwater-bearing aquifers in the area (Grube et al., 2000; Stackebrandt, 1998).

The fault system of the study area consists of four regional fault zones comprising several individual faults. It divides the sedimentary cover of the study area into a regional block structure (Mittenwalde Block; Fig. 1b). The Lausitzer Abbruch and the Fuerstenwalde-Guben fault zones with NW-SE orientation, as well as the Tauer and the Potsdam fault zones striking NE-SW, enclose this compartment. All faults are normal faults with a steep inclination (between 67.8° and 74.3° in average). The Fuerstenwalde-Guben fault zone has a total length of 120 km, and is characterized by an offset of a few hundred metres, whereas the Lausitzer Abbruch fault zone shows displacements up to 1 000 m (Hotzan and Voss, 2013; Beutler and Stackebrandt, 2012; Stackebrandt and Manhenke, 2004).

3 Geological model

We used the Petrel software package (Schlumberger, 2011) for the 3D geological model construction and the subsequent gridding process, and the reservoir simulator TOUGH2-MP/ECO2N for 3D multi-component flow simulations (Pruess, 2005; Zhang et al., 2008). All simulations were conducted on a high performance computing system with 256 cores. Finally, results were imported back into Petrel for visualization purposes.

3.1 Setup

The 3D geological model has a horizontal extent of 100 km × 100 km and a vertical thickness of 1 340 m. It consists of up to three layers: the Rupelian basal sand as the uppermost shallow aquifer, the Muschelkalk Formation as an overlying secondary reservoir and the Detfurth Formation as lowermost reservoir (Fig. 2b). The Rupelian basal sand is 20 m thick and located at a depth of 110 m (Grube et al., 2000). The Lower Muschelkalk Formation is at 1 025 m depth and has a thickness of 140 m, while the reservoir is at 1 425 m depth with a thickness of 23 m (Tillner et al., 2013). Figure 2b shows the geological model with a regular lateral grid resolution of 250 m × 250 m. The vertical discretisation depends on the different model layers, and ranges between 10 m and 19.9 m (Table 2).

In a previous study, Kühn and Kempka (2015) investigated the influence of caprock permeabilities on shallower aquifer salinization at the prospective storage site Beeskow. Their results showed that for caprock permeabilities equal or lower than 10^{-17} m^2 no increase in salt concentration in formations above the reservoir has to be expected. The top formation seal in the study area mainly consists of marine evaporates such as anhydrite and halite with a total thickness of up to 180 m. We therefore defined the caprocks as impermeable for fluid flow in all simulations. Thus, only the faults provide a hydraulic connection between the shallow aquifer and the reservoir. Thereto, the elements of the faults as well as the different reservoir layers were “active” in the simulations, whereby the elements representing the caprocks were not considered.

Within our model only the inner faults, which enclose the Mittenwalde Block were implemented as a representation of the entire fault zone (Fig. 1b). Thereto, fault related parameters were assigned to the elements located at the respective vertical fault plane. The fault element width of 250 m corresponds to the overall lateral grid resolution. This element width is relatively large but still realistic, since all regional fault zones consist of several

individual faults and show considerable displacements between a few hundred meter to 1 000 m. In general, fault offset is linked to the width of the damage zone (Faulkner et al. 2010; Mitchel and Faulkner, 2009; Wibberley et al., 2008). For example, faults with displacements between 10 m and 1 000 m can have damage zone widths between tens and hundreds of metres. However, there exists no simple relationship, since the width of the damage zone is highly dependent on lithology, pressure, temperature, and strain rate during shear and potentially tensile deformation (Shipton et al., 2006). Due to the relatively steep inclination of all faults and to maintain maximum grid regularity, the dip angle was neglected in the present model and all faults were assumed to be strictly vertical. In the following, the Fuerstenwalde-Guben fault zone is addressed as Fault 1. The Potsdam, the Lausitzer Abbruch and the Tauer fault zones are referred to as Faults 2, 3 and 4, respectively (Fig. 1b).

3.2 Parameterization

All lithological units were parameterized according to Tillner et al. (2013) and Vattenfall (2009), with values derived from borehole data and literature and modelled as homogenous and isotropic. The Detfurth Formation has a permeability of 400 mD, while the overlying secondary reservoir (Muschelkalk Formation) is characterized by a permeability of 200 mD (Table 2). Porosity and permeability of the Rupelian basal sand was chosen according to Tesch et al. (1987). Fault permeability was assumed higher than that of the host rock, because of fault-parallel permeability enhancement of the damage zone due to the presence of a fracture network (Jourde et al., 2002; Caine et al., 1996). A lateral barrier to groundwater flow due to a low permeable fault core was not directly considered in the simulations. However, as a conservative approach we assume that hydraulic properties of the fault damage zones are in between those of the Rupelian basal sands and the Detfurth Formation to promote upward brine displacement instead of across fault flow (Table 2).

Because faults have a smaller offset at their boundaries, and consequently a less distinct damage zone, it was presumed that permeability declines in these areas. This was implemented into the model by using permeability multipliers in the respective elements. The permeability declines linearly towards the ends of the fault, applied to the first and last 15 % of its length.

3.3 Initial and boundary conditions

In all investigated scenarios, Dirichlet boundary conditions were applied to the Rupelian basal sand. These were implemented by volume multipliers of 10^{10} at the boundary elements of each layer, so that the aquifer has infinite extension. The boundaries of the Detfurth and the Muschelkalk formations are either open (boundary element volume multiplication by 10^5; quasi-infinite) or closed (no boundary element volume multiplication), depending on the investigated scenario. The higher volume multiplication at the boundary elements of the Tertiary Rupelian basal sand is based on the assumption that a continuous hydraulic connection throughout the formation is more likely in the younger and less consolidated sedimentary deposits than in the more tectonically influenced deeper rocks. For the temperature distribution, a constant geothermal gradient of 30 °C km^{-1} was used, starting from 15 °C at the model top. All simulations were performed at isothermal conditions. Salinity is assumed to increase with depth either by a gradient of 0.23 g kg^{-1} solution per meter from zero at the base of the Rupelian basal sand up to a maximum of 25 % at a depth of 1070 m (Vattenfall, 2009) or sharply from zero in the Rupelian to 25 % below that aquifer. The last conditions were chosen, as they lead to the maximum possible salinization in the uppermost aquifer, and thus represent the most unfavourable scenario for shallow aquifers under the given assumptions.

In the respective industrial project at the Beeskow storage site, it was planned to inject 34 Mt of CO_2 over a time span of 20 years into the Mesozoic formations at the top of an anticline structure (Tillner et al., 2013). In the present study, the equivalent volume of brine was injected into the storage formation instead of CO_2, which enables us to study also the long-term effects of brine displacement more than 1 000 years after the injection stop. Without topographic variations in the reservoir, CO_2 is not immobilized in structural traps (e.g. below an anticline top) and might reach the Fuerstenwalde-Guben fault zone located at a distance of 4 km from the injection well over such a long simulation period, which should not be focus of investigation in the present study. Furthermore, with such a model we keep the findings of injection-related brine displacement transferable to various other types of subsurface storage. All simulations start from hydrostatic pressure conditions. Considering the density of brine, pressure at the top of the Detfurth Formation at 1 425 m depth is approximately 165 bar. At a reservoir temperature of 58 °C, the resulting CO_2 density is 668.5 kg m^{-3} (Span and Wagner, 1996). Taking into account the salinity of 25 % in the reservoir, brine density is 1 175 kg m^{-3}.

Thus, a volume equivalent mass of 59.76 Mt brine was injected into the storage formation, corresponding to a rate of 94.6 kg s^{-1}.

Brine densities are calculated in TOUGH2-MP/ECO2N for each element during the simulation and fluid compressibility is then considered by its density changes. Pore compressibility causes a higher storage coefficient in the formations when pressure increases. Since our simulations should show the greatest possible effect on brine displacement, pore compressibility was neglected. Assuming a fluid diffusion coefficient of 2×10^{-9} m^2 s^{-1} and a sharp freshwater-saltwater interface in the fault, it would take about 1 million years in the present model for the salinity front to propagate into a neighbouring element. We therefore neglected diffusion as well.

4 Set of scenarios

In total, 19 scenarios were selected to investigate the conditions for upward brine flow through the faults. Different fault lengths and permeabilites, hydrogeological boundary conditions and vertical salinity distributions as well as the presence of a secondary reservoir formation above the target storage horizon were considered. Scenarios are identified by the following abbreviations:

$$\boldsymbol{Scenario = F_n^{\,l}\, B_{O/C}\, SR_k}$$

Where *F* denotes fault with the coefficients *l* indicating the total fault length and *n* the number of active faults. Further, the lateral boundary conditions (*B*) of both reservoirs can be either open (*O*) or closed (*C*). *SR* denotes that an overlying secondary reservoir exists and *k* specifies the permeability of that reservoir. Scenarios in which a salinity gradient was applied are marked with *'*'*. All simulated scenarios with their varying initial and boundary conditions are summarized in Table 3 and 4.

The base cases consist of two layers, while three different fault lengths were considered. Either all four fault zones with a total length of 193 km were assumed to be permeable, or Fault 1 was defined to be hydraulically conductive with a length of 60 km. In the third case, only a length of 2 kilometres in the central part of Fault 1 was presumed to be open for fluid flow (Fig. 1b). Based on the effective porosity assumed for all fault zones and the total fault element volumes, the effective damage zone volume for the three different cases can be specified with 1.6×10^{10} m^3 (fault length of 193 km), 4.9×10^{9} m^3 (fault length of 60 km) and

1.8×10^8 m^3 (fault length of 2 km), respectively. For all these cases, scenarios with both open and closed reservoir boundaries as well as an overlying secondary reservoir were examined to illustrate the entire range of a potential freshwater salinization depending on the given geological constraints.

5 Results

Results of injection induced brine displacement via the faults are analysed at 20 years corresponding to the end of the injection period. At this time, reservoir pressures have reached their maximum, and thus effects on upward brine flow are most noticeable. In Sections 5.2 to 5.5, salinity is assumed to increase sharply from zero in the Rupelian basal sand to 25 % below that aquifer. In Section 5.6, the impact of a salinity gradient on shallower aquifer salinization is presented. Here, salinity in the fault(s) increases from zero at the base of the Rupelian up to a maximum of 25 % at a depth of 1 070 m. Fault permeability is 700 mD in all investigated scenarios, except for the comparison presented in Section 5.4, where duration of mass flow and shallow aquifer salinization are investigated also for lower fault permeabilities of 10 mD and 200 mD. In Section 5.5, it is shown how a secondary reservoir with a permeability higher than that of the faults affects upward brine migration.

5.1 General outcomes

In all simulations, an injection-related pattern in pressure distribution and fluid flow can be observed. Figure 3 shows the mass flow of brine as an example for Scenario $F_{1\text{-}4}^{193km}\,B_O$ after 20 years. Starting from the injection location, brine is displaced radially within the reservoir, and hence predominantly into parts of the faults close to the point of injection. However, the course of the four fault zones and the hydraulically conductive fault length impacts fluid flow out of the fault in the shallow aquifer, and thus pressure gradients, so that brine distribution is not symmetric along the faults in the Rupelian basal sand. In case of four open faults, brine that flows out of the faults migrates into the Mittenwalde Block (compartment in the central model domain bounded by the four fault zones; Figure 1) from all four fault zones and towards the open model boundaries. Consequently, pressure gradients are becoming lower in the Mittenwalde Block, so that flow out of all faults towards the lateral boundaries dominates at the final injection stage, since brine is displaced away from the point of highest pressure build-up.

Duration and intensity of fluid flow determine the spatial distribution of displaced brine. In all scenarios, maximum mass flow is observed along Fault 1 close to the injection point decreasing towards the fault edges. This pattern is reflected in the salinization of the freshwater aquifer, as shown in Figure 4a. A maximum salinity in the shallow aquifer is reached at the end of the injection period in the central part of Fault 1, irrespective of whether a sharp salt-/freshwater boundary at the base of the Rupelian (e.g. Scenario $F_{1\text{-}4}^{193km}\,B_C$) or a salinity gradient (Scenario $F_{1\text{-}4}^{193km}\,B_C^{*}$) was applied. Salt concentrations then decrease continuously towards the fault edges by more than 80 %. Salinity levels are generally highest within the lower element layer, indicating that the denser saline water preferably spreads along the base of the aquifer (Fig. 4b). Decreasing upward brine displacement after the injection stop causes a downward flow of the denser saline water, which consequently accumulates at the base of the shallow aquifer. Moreover, a slight backflow into the fault occurs due to the increased weight of the water column. Hence, the salinity in the shallow aquifer slightly decreases after a simulated time of a few hundred years (Fig. 4b).

5.2 Fault length / effective damage zone volume

The impact of the hydraulic conductive fault length on shallow aquifer salinization is presented in the following. We considered total fault lengths of 2 km, 60 km and 193 km, corresponding to an effective damage zone volume of 1.8×10^8 m^3, 4.9×10^9 m^3 and 1.6×10^{10} m^3, respectively (Table 3).

Figure 5a shows that overpressures in the Detfurth Formation are generally highest assuming laterally closed reservoir boundaries. The pressure development at the base of Fault 1 indicates that pressure increases until the injection stop after 20 years (Fig. 5b). In case of a hydraulic conductive fault segment with a length of two kilometres only, brine displacement, and thus pressure dissipation occurs over the smallest area. Consequently, the highest pressure build-up at the injection point (89.9 bar) and the base of Fault 1 (19.0 bar), into which brine is predominantly displaced is observed for Scenario $F_1^{2km}\,B_C$ (Table 3). A greater effective fault damage zone volume reduces the pressure increase at the base of Fault 1 to 12.1 bar (Scenario $F_1^{60km}\,B_C$) and 10.9 bar ($F_{1\text{-}4}^{193km}\,B_C$), respectively. Under the assumption of laterally open reservoir boundaries, pressure increase is reduced by a further 23 % in average compared to all three cases with closed boundaries.

Saline water, migrating into the Rupelian basal sand, originates only from the fault(s) and not from greater depth. The higher the vertical pressure gradient, the greater the depth in the fault from which brine is displaced into the shallow aquifer. Hence, in Scenario $F_1^{2km}\,B_C$ saline water rises into the shallow aquifer from the upper 132 m of the fault, counting from the base of the Rupelian basal sand (Table 3). This maximum displacement depth refers to the central part of Fault 1, where pressure gradients are highest due to the proximity to the injection point. Displacement depths decrease towards the fault edges to partly less than 1 m. The effect of this displacement depth is that the degree in salinization in the Rupelian basal sand becomes locally higher with decreasing effective fault damage zone volume. In Scenario $F_1^{2km}\,B_C$, the average salt mass of the area that is affected by a salt concentration exceeding 0.5 g kg^{-1} solution (hereafter referred to as salinization area), which corresponds to the maximum allowable limit prescribed by the German Drinking Water Ordinance (TrinkwV, 2001), is 312 kg m^{-2} after 20 years. In turn, the total salinization area in the Rupelian basal sand is expectably larger the greater the fault length. In Scenario $F_{1\text{-}4}^{193km}\,B_C$, this area is more than seven times as large as in Scenario $F_1^{2km}\,B_C$ (Table 3). However, the salt mass per unit area is considerably lower, since pressure dissipation occurs over a greater hydraulic conductive fault length, which reduces pressure gradients and brine displacement depths in the faults (30 m in Scenario $F_1^{60km}\,B_C$ and 29 m in Scenario $F_{1\text{-}4}^{193km}\,B_C$). Thus, the average salt mass of the salinization area in the Rupelian basal sand is 141 kg m^{-2} in Scenario $F_1^{60km}\,B_C$ and 84 kg m^{-2} in Scenario $F_{1\text{-}4}^{193km}\,B_C$. Lower vertical pressure gradients in the fault in case of laterally open reservoir boundaries reduce brine displacement depths and flow velocities out of the faults, respectively, and consequently the size of the salinization areas and average displaced salt masses in the Rupelian basal sand compared to the scenarios with closed reservoir boundaries (Fig. 6).

After the injection stop, fluid flow persists until the overpressure in the storage formation is completely reduced. Duration of fluid flow and pressure reduction thereby depend on the lateral boundary conditions and the hydraulically conductive fault length. Pressure reduces substantially faster with increasing fault length and under the assumption of laterally open fluid flow boundaries that allow for horizontal brine displacement across the model boundaries (Fig. 5b). Hence, the duration of brine displacement into the shallow aquifer is shorter for all three scenarios. After 31 years (Scenario $F_1^{2km}\,B_O$) to 42 years (Scenario $F_{1\text{-}4}^{193km}\,B_O$), pressure conditions prior to injection are re-established (Fig. 7a). In case of

closed reservoir boundaries, pressure reduction in the incompressible domain solely comes from vertical brine displacement via the fault(s) towards the laterally infinite shallow aquifer. Thus, under the assumption of a sharp salt-freshwater boundary, the mass of salt displaced into the shallow aquifer corresponds to the overall injected salt mass (Fig. 7b). In this case, the open fault length affects only the duration of fluid migration, which can be between 66 years (Scenario $F_{1\text{-}4}^{193km}\,B_C$) and 330 years (Scenario $F_1^{2km}\,B_C$); (Fig. 7a). Decreasing vertical pressures after upward brine migration stops at the end of injection, cause a slight backward flow of brine out of the shallow aquifer and back into the fault in case of a small effective fault damage zone volume and laterally open reservoir boundaries. Over a period of 300 years, the average salt mass in the Rupelian decreases by about 7.5 x 10^8 kg salt (Scenario $F_1^{2km}\,B_O$).

5.3 Overlying secondary reservoir

A secondary reservoir above the storage formation also hydraulically connected to the fault zones has a strong impact on pressure build-up within the injection horizon, and hence vertical pressure gradients in the fault(s). If reservoir boundaries are closed for fluid flow, the pressure increase at the base of Fault 1 ranges from 9.0 bar ($F_1^{2km}\,B_C\,SR_{200mD}$) to 6.4 bar ($F_{1\text{-}4}^{193km}\,B_C\,SR_{200mD}$), which corresponds to 48 % and 59 % of the pressure increase, respectively, without considering the overlying secondary reservoir. Under the assumption of laterally open reservoir boundaries, pressure increase is again reduced by further 24 % in average, compared to all three cases with secondary reservoir and closed boundaries. This results in the lowest vertical pressure gradients in the fault(s) observed in the present scenario analysis. Lower reservoir pressures due to an overlying secondary reservoir induce lower flow velocities out of the fault as well as shown in Figure 8. Moreover, brine displaced into the Rupelian basal sand originates from considerably shallower depths in the fault. Here, brine is displaced into the Rupelian basal sand from the upper 70 m of Fault 1 in Scenario $F_1^{2km}\,B_C\,SR_{200mD}$ and 17 m in Scenario $F_{1\text{-}4}^{193km}\,B_C\,SR_{200mD}$ considering laterally closed reservoir boundaries. Under the assumption of open flow boundaries, brine mainly originates from the upper 56 m (Scenario $F_1^{2km}\,B_O\,SR_{200mD}$) and 16 m (Scenario $F_{1\text{-}4}^{193km}\,B_O\,SR_{200mD}$) of the faults only. Consequently, the area affected by a salt concentration exceeding 0.5 g kg^{-1} solution in the Rupelian basal sand as well as the average salt mass in the salinization area are reduced by about one third compared to the respective scenario without considering a

secondary reservoir (Table 3). Again, pressure conditions prior to injection re-establish fast after the injection stop and under the assumption of laterally open reservoir boundaries (e.g., 40 years for Scenario $F_1^{60km}\ B_O\ SR_{200mD}$); (Fig. 9). In turn, the reduction of the comparatively lower overpressures takes significantly more time in case of laterally closed reservoir boundaries, e.g., the mass flow into the Rupelian basal sand continuous for about 225 years ($F_{1\text{-}4}^{193km}\ B_C\ SR_{200mD}$) and 1 050 years ($F_1^{2km}\ B_C\ SR_{200mD}$), which is more than three times longer compared to the models without a secondary reservoir (Fig. 10). This retardation in fluid flow is attributable to the fact that the overpressure in both, injection horizon and secondary reservoir is successively reduced after the injection stop. According to the pressure gradient towards the Rupelian basal sand with laterally infinite extension, brine is displaced out of the secondary reservoir again after the injection stop and into the shallow aquifer (Fig. 11). Thus, the overall displaced salt mass in the shallow aquifer is almost identical compared to the corresponding scenarios without secondary reservoir, when pressure comes to an equilibrium (Fig. 10).

5.4 Fault permeability

To evaluate the impact of fault permeability on upward brine displacement via the existing faults, a comparison was made between six scenarios that consider an effective damage zone volume of 1.6 x 10^{10} m^3 (total fault length of 193 km) and a fault permeability of 10 mD, 200 mD and 700 mD for laterally open and closed reservoir boundaries, respectively. Figure 12 and Table 4 show that the relative salt mass change in the Rupelian basal sand at the injection stop is almost identical for a fault permeability of 700 mD and 200 mD. Thereby, laterally open model boundaries reduce the average salt mass of the salinization areas in the Rupelian basal sand by about 12 % compared with the models using laterally closed boundaries. A less permeable fault with a permeability of 10 mD has a more significant impact on the degree of upper aquifer salinization. The relative salt mass change in the Rupelian basal sand after 20 years is 17 % lower in average compared with a fault permeability of 200 mD or 700 mD. However, in a laterally closed and incompressible domain all the pressure relief comes from upward brine migration. Consequently, all the injected brine volume reaches the shallow aquifer after a certain time since flow persists until the overpressure in the storage formation is completely reduced. In this case, a low-permeable fault only extends the duration of mass flow into the shallow aquifer, which can persist up to

310 years (Fig. 12; Table 4). At that time, the total salt mass displaced into the Rupelian basal sand is the same as for the scenarios with a fault permeability of 200 mD or 700 mD.

5.5 Permeability difference between fault and secondary reservoir

Our simulations demonstrate that if reservoir boundaries are closed, the permeability of the fault primarily influences the duration of fluid flow. After a certain period, the overall displaced salt mass into the freshwater aquifer becomes equal, if fault zones are sufficiently permeable. For this case, it is irrelevant if fault permeability is higher, equal or lower compared to the reservoir or aquifer. This is not true for open reservoir flow boundaries (infinite aquifer). In Scenario $F_{1\text{-}4}^{193km}\, B_O\, SR_{2000mD}$, the permeability of the Muschelkalk Formation is distinctly higher than that of the fault. The pressure increase at the base of Fault 1 is only 1.2 bar, which corresponds to 23 % of the total pressure increase, considering a Muschelkalk Formation permeability of 200 mD ($F_{1\text{-}4}^{193km}\, B_O\, SR_{200mD}$). In consequence, brine that is displaced into the shallow aquifer originates solely from the upper 4 m of the faults. This results in the smallest salinization area and the lowest degree in salinization in the Rupelian basal sand compared to all other scenarios with a sharp salt-/freshwater boundary (Fig. 13; Table 3). In addition, the shortest duration of mass flow into the Rupelian basal sand with only 23 years is observed for Scenario $F_{1\text{-}4}^{193km}\, B_O\, SR_{2000mD}$.

5.6 Salinity gradient

Two further scenarios, considering a total fault length of 2 km (Scenario $F_1^{2km}\, B_C^{*}$) and 193 km (Scenario $F_{1\text{-}4}^{193km}\, B_C^{*}$), without an overlying secondary reservoir and laterally closed reservoir boundaries were employed to investigate the impact of a salinity gradient on the degree of shallow aquifer salinization. The pressure increase at the base of Fault 1 is almost identical comparing both scenarios with the corresponding scenario exhibiting a sharp salt-/freshwater boundary below the Rupelian. Thus, a significant difference in the brine displacement depth in the faults cannot be observed after 20 years (Table 3). The displacement depth in the fault(s) is 132 m for Scenario $F_1^{2km}\, B_C^{*}$ and 29 m for Scenario $F_{1\text{-}4}^{193km}\, B_C^{*}$, respectively. Consequently, the mass of brine displaced into the shallow aquifer after 20 years is very similar with 2.2 x 10^{10} kg (Scenario $F_1^{2km}\, B_C^{*}$) and 2.5 x 10^{10} kg (Scenario $F_1^{2km}\, B_C$), as well as 4.1 x 10^{10} kg (Scenario $F_{1\text{-}4}^{193km}\, B_C^{*}$) and 4.9 x 10^{10} kg (Scenario $F_{1\text{-}4}^{193km}\, B_C$). However, salt concentrations of brine that is displaced out of the fault(s) and into the shallow aquifer are significantly lower when taking into account a salinity

gradient instead of a sharp salt-/freshwater interface. Hence, the average salt mass of the salinization area in the Rupelian basal sand is only 9 % (Scenario $F_1^{2km}\,B_C^{*}$) and 12 % (Scenario $F_{1\text{-}4}^{193km}\,B_C^{*}$) of that in the respective scenarios with the sharp salt-/freshwater boundary (Fig. 14; Table 3).

6 Discussion

The present study demonstrates how the presence of regional faults can affect upward brine displacement and the degree of shallow aquifer salinization in geological underground utilization. Different fault permeabilites, effective damage zone volumes, hydrogeological boundary conditions and vertical salinity distributions as well as the presence of a secondary reservoir formation above the target storage horizon are considered in a comprehensive large-scale scenario analysis. A 3D geological model of a potential onshore storage site in the Northeast German Basin serves as the basis for this research. The results emphasize that maximum vertical pressure gradients in faults are observed for closed reservoir boundaries, if no overlying secondary reservoir exists and the effective fault damage zone volume is relatively small. The higher the vertical pressure gradient, the greater the depth in the faults from which brine is displaced into the shallow aquifer. A large effective fault damage zone volume, open reservoir boundaries and a secondary reservoir above the storage formation, also hydraulically connected to the fault zones, significantly reduce pressure gradients, and thus displacement depths in the fault. These range between 132 m (Scenario $F_1^{2km}{}_{BC}$) and 4 m ($F_{1\text{-}4}^{193km}\,B_O\,SR_{2000mD}$) after 20 years of fluid injection, respectively. Consequently, salt concentrations in the shallow aquifer are higher in the fault vicinity, the smaller the effective fault damage zone volume. The degree in salinization thereby strongly depends on the initial salinity distribution in the fault. If salinity increases sharply from, e.g., zero in the shallow aquifer to 25 % below its base, the average salt mass of the area affected by salinization amounts to 312 kg m^{-2} after 20 years of injection (Scenario $F_1^{2km}{}_{BC}$). A salinity gradient of 0.23 g kg^{-1} solution per meter reduces the average salt masses of the salinization area in the shallow aquifer by more than 90 % to 28 kg m^{-2} (Scenario $F_1^{2km}{}_{BC}^{*}$). On the contrary, the salinization area in the shallow aquifer, assuming a total hydraulically conductive fault length of 193 km is seven times larger than for a fault length of 2 km. However, lower pressure gradients and brine displacement depths in the fault decrease the degree in salinization in the shallow aquifer, since pressure dissipation occurs over a larger area.

In all scenarios, salinization in the shallow aquifer was observed only along and in close proximity to the open fault zones up to a lateral extent of 2 km (Scenario $F_1{}^{2km}{}_{BC}$; small effective fault damage zone volume) to a few hundred meters ($F_{1\text{-}4}{}^{193km}\, B_O\, SR_{200mD}$; large effective fault damage zone volume and secondary reservoir) from the fault. Brine that reaches the shallow groundwater system spreads preferentially at the aquifer base, as indicated by considerably higher salinities at the lower element layer in our simulations, which is in good agreement with the findings of Oldenburg and Rinaldi (2011). Oldenburg and Rinaldi (2011) further show that upward flux into the bottom-most part of the shallow aquifer is sustained until a new hydrostatic equilibrium is reached, if the pressure elevation is high enough and the dense brine can spread unhindered in the upper aquifer. Our simulation results based on closed reservoir boundaries confirm these results. The mass of brine displaced into the shallow aquifer corresponds to the overall injected mass after several tens to hundreds years, since the duration of brine displacement into the shallow aquifer is not limited to the injection period only. Laterally open reservoir boundaries and a large effective fault damage zone volume support a fast pressure reduction, however brine displacement into the shallow aquifer persists for more than twice the injection period. Under the assumption of closed reservoir boundaries, all pressure relief results from upward brine migration via the faults. In this case, a small effective fault damage zone volume or a low permeable fault only extend the duration of brine flow into shallower units, so that fluid flow can persist for more than 1 000 years until the overpressure in the storage formation is completely reduced, resulting in an ongoing salinization far beyond the time of the injection stop. This demonstrates the relevance of considering also the post-injection phase in salinization assessments, since neglecting the ongoing fluid flow processes could lead to an underestimation of the potential freshwater salinization. Nevertheless, it should be noted that regional groundwater flow and mixing with local recharge would probably have a strong effect on the reduction of salt concentrations in the shallow aquifer over a period of several hundred years. As demonstrated by the results, it is crucial to represent the site-specific geological conditions as close as possible. Cavanagh and Wildgust (2011) point out that storage formations are unlikely to have zero-flow boundaries and are rather open with respect to single-phase flow and pressure dissipation via brine displacement at regional scale.

In a previous study focussing on the same storage site, Tillner et al. (2013) demonstrated that increasing fault permeability from 100 mD to 10 000 mD does not significantly affect the

degree in shallow aquifer salinization. Our simulations further show that only low fault permeability has a significant impact on upward brine migration. Depending on the lateral reservoir boundaries, the relative salt mass change in the shallow aquifer after 20 years is 13-22 % lower for a fault permeability of 10 mD compared with a fault permeability of 700 mD. Tillner et al. (2013) mainly considered fault permeabilities higher than that of the reservoir and overlying permeable formations. Our simulations demonstrate that the preferential brine flow direction, and thus salinization of upper aquifers is determined by the permeability contrast between fault and reservoir and/or overlying secondary reservoirs. If permeability of an overlying secondary reservoir exceeds that of the fault ($F_{1\text{-}4}^{193km}\ B_O\ SR_{2000mD}$), the mass of brine migrating into the shallow aquifer is only around a quarter of that observed in the opposite case ($F_{1\text{-}4}^{193km}\ B_O\ SR_{200mD}$). Thus, it can be concluded that in multi-barrier systems the potential salinization of a shallow aquifer is lowered with each intermediate aquifer, if a hydraulic connection exists between the fault or leakage pathway and that aquifer. Similar results were achieved by an analytical approach of Nordbotten et al. (2004), investigating fluid leakage through wells in a multi-barrier system with up to twelve aquifers. The authors observed a successive decrease in the intensity of upward fluid displacement, caused by the migration of fluid into the intermediate aquifer layers, consequently reducing fluid migration in the shallowest aquifer. Birkholzer et al. (2009) also showed that the amount of fluid displaced into formations above the reservoir decreases in upward direction due to the attenuation capacity of the overlying rocks; however, without considering a vertical conduit. Further, Walter et al. (2012) concluded that saltwater intrusion into potable groundwater resulting from geological CO_2 storage in a saline aquifer occurs most likely in the vicinity of vertical fluid conduits and not over large areas, if sites with multi barrier systems and intermediate aquifers are selected. Zeidouni (2012) evaluated vertical communication between aquifers through a leaky fault by an analytical approach and showed that the attenuation capacity of a single, thick overlying aquifer is distinctly smaller than that of a multi-layered system.

In the present study, a conservative modelling approach in the assessment of potential upper aquifer salinization by upward brine migration from saline formations was chosen. We injected brine instead of CO_2 and neglected pore compressibility in our models to maximize pressurization and related brine displacement. Considering the effects of CO_2 and/or pore compressibility, would induce a lower injection-related pressure-build up due to higher

storage coefficients, and consequently to less intense brine displacement in the injection period. Furthermore, our simulations with a fault fully saturated with brine correspond to an end member resulting in maximum freshwater salinization. Brine migration across the faults is possible, since no impermeable fault core was considered; however, brine migration occurs almost solely upward into the overlying formations and is negligible in horizontal direction across the faults, when applying a higher fault than reservoir permeability. Hence, the presented modelling results are valid for one specific fault architecture promoting vertical fluid flow, as a least favourable case with respect to shallow aquifer salinization. In multi-layer systems with alternating layers of reservoirs and caprocks, as that considered in the present study, fault permeability within the caprock layers is usually lower than that of the fault host rocks resulting from the clay smearing effect (e.g. Crawford et al., 2008; Egholm et al., 2008). Fault permeability varies not only with mineralization along the fault plane, but also with e.g., depth, fault throw and orientation, inducing highly heterogeneous horizontal and vertical permeability patterns (e.g., Vilarrasa and Carrera, 2015; Bense and Person, 2006; Odling et al., 2004; Shipton et al., 2003; Fisher and Knipe, 2001). Heterogeneity in fault permeability can prevent brine from migrating in upward direction and result in much lower salt concentrations or a differently distributed salinization pattern in the shallow aquifer as presented here. However, hydraulic properties and the spatial extent of fault damage zones are difficult to detect and therefore exhibit a high uncertainty in predicting fault fluid flow and potentially resulting shallow freshwater salinization (Odling et al., 2004; Harris et al., 2003). Further, geomechanical effects are relevant in the assessment of fault fluid flow and several authors have explored the impact of injection-induced pressure build-up on fault zones stability (e.g., Kempka et al., 2015; Rinaldi et al., 2015; Tillner et al., 2014; Magri et al., 2013; Röhmann et al., 2013; Cappa and Rutqvist, 2011). For this purpose, coupled hydro-mechanical simulations are applied to account for the interaction between hydraulic and mechanical processes, potentially triggering fault slip and dilation resulting in, e.g., new or enhanced leakage pathways for formation fluids. To minimize pressure perturbation due to fluid injection, and thus fault fluid flow, simultaneous fluid injection and production from storage reservoirs is discussed as one efficient mitigation measure to be applied in geological underground utilization (Kempka et al., 2014; Tillner et al., 2013; Court et al., 2012; Bergmo et al., 2011; Buscheck et al., 2011).

For future investigations, we extend the assumptions made in the present study by the implementation of heterogeneous fault zones with spatial variations in porosity and permeability as well as related non-uniform architecture and fault inclination. Furthermore, research is underway to implement the 3D model presented here in coupled hydro-mechanical simulations to account for potential fault shear failure and permeability changes that may alter fault fluid flow.

7 Summary and Conclusions

A regional scale 3D model of the prospective storage site Beeskow in the Northeast German Basin was implemented to investigate the potential salinization of potable groundwater resources, resulting from upward brine migration through hydraulically conductive fault zones. For that purpose, 19 scenarios were examined to assess the impact of fault lengths between 2 km and 193 km in the vicinity and around the injection location. Further, the effects of an overlying secondary reservoir, hydrogeological boundary conditions and the initial salinity distribution on freshwater salinization were evaluated. We demonstrate that pressure build-up and development within the reservoir determine the intensity and duration of fluid flow through the faults and shallow aquifer salinization, mainly controlled by the lateral model boundary settings and the effective fault damage zone volume. In general, the potential of freshwater salinization is low for greater effective fault damage zone volumes or fault lengths, because the origin depth of the fluids displaced into the shallow aquifer is located a few decametres below the shallow aquifer in maximum due to relatively low vertical pressure gradients. Short and very permeable fault segments or a small effective fault damage zone may result in a higher salinization potential due to a larger vertical fault height affected by fluid displacement. The degree in shallow aquifer salinization thereby strongly depends on the initial salinity distribution in the investigated area and especially that in the fault. If a gradient in salinity exists or the salt-freshwater interface lies below the fluid displacement depth in the faults, freshwater salinization is considerably lower compared to scenarios with a sharp freshwater-brine interface located directly below the shallow freshwater aquifer. Moreover, it can be concluded that intermediate aquifers lying in between the storage reservoir and the shallow freshwater aquifer, further diminish salinization in the shallow aquifer, because brine originating from the faults is partly displaced into these intermediate layers. Lateral boundary conditions mainly influence the duration of brine displacement:

while open reservoir boundaries allow for fast pressure dissipation, fluid flow persists for several hundred to a thousand years in a spatially restricted reservoir until the mass of brine displaced into the shallow aquifer corresponds to the overall injected fluid mass (assuming zero pore compressibility). Considering our simulation results, we conclude that hydraulically conductive fault zones do not necessarily lead to freshwater salinization owing to upward brine displacement. This principally depends on the initial salinity distribution, effective volume of the fault damage zone and the hydrogeological boundary conditions.

We demonstrated how to apply numerical simulations to provide site-specific insights on the relevant factors affecting dynamic fluid flow processes and brine displacement into shallow freshwater aquifers. Since most storage sites are very complex from the geological point of view, and especially the spatial distribution of heterogeneities in the subsurface at the regional scale is not well known, we focused here on selected parameter end members to estimate the site-specific bandwidth of potential freshwater salinization. Field explorations have to be employed prior to any underground utilization to obtain the most accurate data, especially on hydraulic properties of existing fault zones as well as the initial salinity distribution.

Acknowledgements

We would like to thank our colleagues Benjamin Nakaten and Marco De Lucia (GFZ German Research Centre for Geosciences) for technical support and constructive comments.

References

Bense, V.F. and Person, M.A.: Faults as conduit-barrier systems to fluid flow in siliciclastic sedimentary aquifers, Water Resour. Res., 47 (W05421), 1-18, doi:10.1029/2005WR004480, 2006.

Bergmo, P.E.S., Grimstad, A.-A. and Lindeberg, E.: Simultaneous CO_2 injection and water production to optimise aquifer storage capacity, Int. J. Greenh. Gas Con., 5 (3), 555-564, doi:10.1016/j.ijggc.2010.09.002, 2011.

Beutler, G. and Stackebrandt, W.: Der Schollenbau des Tafeldeckgebirges von Brandenburg – Vorschlag für eine einheitliche Benennung [The tectonic pattern of the sedimentary cover of Brandenburg – suggestion for a uniform nomenclature], Brandenburgische Geowissenschaftliche Beiträge, 19 (1), 93-109, 2012.

Birkholzer, J.T., Zhou, Q. and Tsang, C.-F.: Large-scale impact of CO_2 storage in deep saline aquifers: a sensitivity study on pressure response in stratified systems, Int. J. Greenh. Gas Con., 3, 181-194, doi:10.1016/j.ijggc.2008.08.002, 2009.

Birkholzer, J.T., Nicot, J.P., Oldenburg, C.M., Zhou, Q., Kraemer, S. and Bandilla, K.: Brine flow up a well caused by pressure perturbation from geologic carbon sequestration: static and dynamic evaluations, Int. J. Greenh. Gas Con., 5, 850-861, doi:10.1016/j.ijggc.2011.01.003, 2011.

Buscheck, T.A., Sun, Y., Hao, Y., Wolery, T.J., Bourcier, W., Tompson, A. F.B., Jones, E.D., Friedmann, S.J. and Aines R.D.: Combining brine extraction, desalination, and residual-brine reinjection with CO_2 storage in saline formations: Implications for pressure management, capacity, and risk mitigation, Energy Procedia, 4, 4283-4290 doi:10.1016/j.egypro.2011.02.378, 2011.

Caine, J., Evans, J. and Forster, C.: Fault zone architecture and permeability structure, Geology, 24 (11), 1025-1028, doi:10.1130/0091-7613(1996)024<1025:FZAAPS>2.3.CO;2, 1996.

Cappa, F. and Rutqvist, J.: Modeling of coupled deformation and permeability evolution during fault reactivation induced by deep underground injection of CO_2, Int. J. Greenh. Gas Con., 5, 336-346, doi:10.1016/j.ijggc.2010.08.005, 2011.

Cavanagh, A. and Wildgust, N.: Pressurization and brine displacement issues for deep saline formation CO_2 storage, Energy Procedia, 4, 4814-4821, doi:10.1016/j.egypro.2011.02.447, 2011.

Chin, L.Y., Raghavan, R. and Thomas, L.K.: Fully coupled geomechanics and fluid-flow analysis of wells with stress-dependent permeability, SPE J., 5 (1), 32-45, Paper 58968, doi:10.2118/58968-PA, 2000.

Chiaramonte, L., Zoback, M. D., Friedmann, S. J. and Stamp V.: Seal integrity and feasibility of CO_2 sequestration in the Teapot Dome EOR Pilot: Geomechanical site characterization, Environ. Geol., 54 (8), 1667-1675, doi:10.1007/s00254-007-0948-7, 2008.

Court, B., Bandilla, K.W., Celia, M.A., Buscheck, T.A., Nordbotten, J.M., Dobossy, M. and Janzen, A.: Initial evaluation of advantageous synergies associated with simultaneous brine production and CO_2 geological sequestration, Int. J. Greenh. Gas Con., 8, 90-100, doi:10.1016/j.ijggc.2011.12.009, 2012.

Crawford, B.R., Faulkner, D.R, and Rutter, E.H.: Strength, porosity, and permeability development during hydrostatic and shear loading of synthetic quartz-clay fault gouge, J. Geophys. Res.-Sol. Ea., 113, B03207, doi:10.1029/2006JB004634, 2008.

Dempsey, D., Kelkar, S. and Pawar, R.: Passive injection: A strategy for mitigating reservoir pressurization, induced seismicity and brine migration in geologic CO_2 storage, Int. J. Greenh. Gas Con., 28, 96-113, doi:10.1016/j.ijggc.2014.06.002, 2014.

Egholm, D.L., Clausen, O.R., Sandiford, M., Kristensen, M.B. and Korstgård, J.A.: The mechanics of clay smearing along faults, Geology, 36 (10), 787-790, doi:10.1130/G24975A.1, 2008.

Faulkner, D.R., Jackson, C.A.L., Lunn, R.J., Schlische, R.W., Shipton, Z.K., Wibberley, C.A.J. and Withjack, M.O.: A review of recent developments concerning the structure, mechanics and fluid flow properties of fault zones, J. Struct. Geol., 32, 1557-1575, doi:10.1016/j.jsg.2010.06.009, 2010.

Fisher, Q.J. and Knipe, R.J.: The permeability of faults within siliciclastic petroleum reservoirs of the North Sea and Norwegian Continental Shelf, Mar. Petrol. Geol., 18 (10), 1063-1081, doi:10.1016/S0264-8172(01)00042-3, 2001.

Forster, C.B. and Evans, J.P.: Fluid flow in thrust faults and crystalline thrust sheets: Results of combined field and modeling studies, Geophys. Res. Lett., 18, 979-982, 1991.

Grube, A., Wichmann, K., Hahn, J. and Nachtigall, K.: Geogene Grundwasserversalzung in den Poren-Grundwasserleitern Norddeutschlands und ihre Bedeutung für die Wasserwirtschaft, DVGW-Technologiezentrum Wasser, Band 9, Karlsruhe, 2000.

Hannemann, M. and Schirrmeister, W.: Paläohydrogeologische Grundlagen der Entwicklung der Süß-/Salzwassergrenze und der Salzwasseraustritte in Brandenburg [Paleohydrological basics of the development of the boundary of fresh and salt water as well as of the salt water-outlets in Brandenburg], Brandenburgische Geowissenschaftliche Beiträge, 5 (1), 61-72, 1998.

Harris, S.D, McAllister, E., Knipe, R.J. and Odling, N.E.: Predicting the three-dimensional population characteristics of fault zones: a study using stochastic models, J. Struct. Geol., 25 (8), 1281-1299, doi:10.1016/S0191-8141(02)00158-X, 2003.

Hotzan, G. and Voss, T.: Komplexe hydrogeochemisch-genetische Kartierung zur Einschätzung der Salzwassergefährdung pleistozäner und tertiärer Grundwasserleiter im Raum Storkow-Frankfurt (Oder)-Eisenhüttenstadt [Complex hydrogeochemic-genetic mapping for evaluation of the endangerment of pleistocene and tertiary aquifers by saline waters in the region Storkow-Frankfurt (Oder)-Eisenhüttenstadt], Brandenburgische Geowissenschaftliche Beiträge, 20 (1/2), 62-82, 2013.

IEA Greenhouse Gas R&D Programme (IEA GHG): CCS Site Characterization Criteria, Technical Study, Report No. 2009/10, 130 pp. 2008.

IPCC - Metz, B., Davidson, O., de Coninck, H.C., Loos, M. and Meyer L.A. (Eds.): IPCC Special Report on Carbon Dioxide Capture and Storage, Prepared by Working Group III of the Intergovernmental Panel on Climate Change, Cambridge University Press, New York, 431 pp., 2005.

Jourde, H., Flodin, E., Aydin, A., Durlovsky, L. and Wen, X.: Computing permeability of fault zones in eolian sandstone from outcrop measurements, AAPG Bull., 86 (7), 1187-1200, doi:10.1306/61EEDC4C-173E-11D7-8645000102C1865D, 2002.

Kempka, T., Nielsen, C.M., Frykman, P., Shi, J.-Q., Bacci, G. and Dalhoff, F.: Coupled Hydro-Mechanical Simulations of CO_2 Storage Supported by Pressure Management

Demonstrate Synergy Benefits from Simultaneous Formation Fluid Extraction, Oil Gas Sci. Technol., 70 (4), 599-613, doi:10.2516/ogst/2014029, 2015.

Kempka, T., Herd, R., Huenges, E., Endler, R., Jahnke, C., Janetz, S., Jolie, E., Kühn, M., Magri, F., Meinert, P., Moeck, I., Möller, M., Muñoz, G., Ritter, O., Schafrik, W., Schmidt-Hattenberger, C., Tillner, E., Voigt, H.-J. and Zimmermann, G.: Joint Research Project Brine: Carbon Dioxide Storage in Eastern Brandenburg: Implications for Synergetic Geothermal Heat Recovery and Conceptualization of an Early Warning System Against Freshwater Salinization. In: Liebscher, A. and Münch, U. (Eds.), Geological Storage of CO_2 – Long Term Security Aspects. GEOTECHNOLOGIEN Science Report No.22, Advanced Technologies in Earth Sciences, Springer International Publishing, 139-166, 2015.

Kempka, T., Klapperer, S. and Norden, B.: Coupled hydro-mechanical simulations demonstrate system integrity at the Ketzin pilot site for CO_2 storage. In: Alejano, L., Perucho, A., Olalla, C. and Jiménez, R. (Eds.), Rock Engineering and Rock Mechanics: Structures in and on Rock Masses; Proceedings of EUROCK 2014, ISRM European Regional Symposium, Leiden: CRC Press/Balkema, 1317-1322, 2014.

Kühn, M. and Kempka, T.: CO_2 Pressurisation of a Storage Reservoir does not Lead to Salinization of Shallower Aquifers through Intact Caprocks, Energy Procedia, 76, 607-615, doi:10.1016/j.egypro.2015.07.880, 2015.

Magri, F., Tillner, E., Wang, W., Watanabe, N., Zimmermann, G. and Kempka, T.: 3D Hydro-mechanical Scenario Analysis to Evaluate Changes of the Recent Stress Field as a Result of Geological CO_2 Storage, Energy Procedia 40, 375-383, doi:10.1016/j.egypro.2013.08.043, 2013.

Mitchell, T. and Faulkner, D.: The nature and origin of off-fault damage surrounding strike-slip fault zones with a wide range of displacements: A field study from the Atacama fault system, northern Chile, J. Struct. Geol., 31 (8), 802-816, doi:10.1016/j.jsg.2009.05.002, 2009.

Nakaten, B., Tillner, E. and Kempka, T.: Virtual Elements for Representation of Faults, Cracks and Hydraulic Fractures in Dynamic Flow Simulations, Energy Procedia, 40, 447-453, doi:10.1016/j.egypro.2013.08.051, 2013.

Nicot, J.: Evaluation of large-scale CO_2 storage on fresh-water sections of aquifers: An example from the Texas Gulf Coast Basin, Int. J. Greenh. Gas Con., 2 (4), 582-593, doi:10.1016/j.ijggc.2008.03.004, 2008.

Nordbotten, J. M., Celia, M. A. and Bachu, S.: Analytical solutions for leakage rates through abandoned wells, Water Resour. Res., 40, W04204, doi:10.1029/2003WR002997, 2004.

Person, M., Banerjee, A., Rupp, J., Medina, C., Lichtner, P., Gable, C., Pawar, R., Celia, M., McIntosh, J. and Bense, V.: Assessment of basin-scale hydrologic impacts of CO_2 sequestration, Illinois basin, Int. J. Greenh. Gas Con., 4 (5), 840-854, doi:10.1016/j.ijggc.2010.04.004, 2010.

Odling, N.E., Harris, S.D. and Knipe, R.J.: Permeability scaling properties of fault damage zones in siliclastic rocks, J. Struct. Geol., 26 (9), 1727-1747, doi:10.1016/j.jsg.2004.02.005, 2004.

Oldenburg, C.M. and Rinaldi, A.P.: Buoyancy Effects on Upward Brine Displacement caused by CO_2 Injection, Transport Porous. Med., 87 (2), 525-550, doi:10.1007/s11242-010-9699-0, 2011.

Pruess, K.: ECO2N: A TOUGH2 Fluid Property Module for Mixtures of Water, NaCl, and CO_2, Lawrence Berkeley National Laboratory, Berkeley, CA, 66 pp., 2005.

Rinaldi, A.P., Vilarrasa, V., Rutqvist, J. and Cappa, F.: Fault reactivation during CO_2 sequestration: effects of well orientation on seismicity and leakage. Greenhouse Gases: Science and Technology, 5 (5), 645-656, doi:10.1002/ghg.1511, 2015.

Röhmann, L., Tillner, E., Magri, F., Kühn, M. and Kempka, T.: Fault Reactivation and Ground Surface Uplift Assessment at a Prospective German CO_2 Storage Site. Energy Procedia 40, 437-446, doi:10.1016/j.egypro.2013.08.050, 2013.

Schlumberger: Petrel Seismic-to-Evaluation Software, Version 2011.2.7, 2011.

Shipton, Z.K. and Cowie, P.A.: A conceptual model for the origin of fault damage zone structures in high-porosity sandstone, J. Struct. Geol., 25, 333-344, doi:10.1016/S0191-8141(02)00037-8, 2003.

Shipton, Z.K., Soden, A., Kirkpatrick, J., Bright, A. and Lunn, R.: How Thick is a Fault? Fault Displacement-Thickness Scaling Revisited. In: Abercrombie, R., McGarr, A., Di Toro,

G., Kanamori, H. (Eds.), Earthquakes: Radiated Energy and the Physics of Faulting, American Geophysical Union, Washington DC, 193-198, doi:10.1029/170GM19, 2006.

Span, R. and Wagner, W.: A New Equation of State for Carbon Dioxide Covering the Fluid Region from the Triple-Point Temperature to 1100 K at Pressures up to 800 MPa, J. Phys. Chem. Ref. Data, 25 (6), 1509-1596, doi:10.1063/1.555991, 1996.

Stackebrandt, W.: Grundzüge des geologischen Baus von Brandenburg [Outline of the geological setting of Brandenburg], Brandenburgische Geowissenschaftliche Beiträge, 5 (2), 3-7, 1998.

Tesch, J., Burmann, G., Schwamm, G. and Nillert, P.: Hydrogeologischer Ergebnisbericht mit Grundwasservorratsberechnung, Vorerkundung Fürstenwalde, VEB Hydrogeologie Nordhausen, BT Berlin, 1-309, Berlin, 1987 (unpublished).

Tillner, E., Shi, J.-Q., Bacci, G., Nielsen, C.M., Frykman, P., Dalhoff, F. and Kempka, T.: Coupled Dynamic Flow and Geomechanical Simulations for an Integrated Assessment of CO_2 Storage Impacts in a Saline Aquifer, Energy Procedia, 63, 2879-2893, doi:10.1016/j.egypro.2014.11.311, 2014.

Tillner, E., Kempka, T., Nakaten, B. and Kühn, M.: Geological CO_2 Storage Supports Geothermal Energy Exploitation: 3D Numerical Models Emphasize Feasibility of Synergetic Use, Energy Procedia, 37, 6604-6616, doi:10.1016/j.egypro.2013.06.593, 2013.

Tillner, E., Kempka, T., Nakaten, B. and Kühn, M.: Brine migration through fault zones: 3D numerical simulations for a prospective CO_2 storage site in Northeast Germany, Int. J. Greenh. Gas Con., 19, 689-703, doi:10.1016/j.ijggc.2013.03.012, 2013.

Trinkwasserverordnung – TrinkwV 2001: Verordnung über die Qualität von Wasser für den menschlichen Gebrauch vom 21.05.2001 (BGBl. I S. 959). Trinkwasserverordnung in der Fassung der Bekanntmachung vom 2. August 2013 (BGBl. I S. 2977), die durch Artikel 4 Absatz 22 des Gesetzes vom 7. August 2013 (BGBl. I S. 3154) geändert worden ist.

Vattenfall: Antrag auf Erteilung einer Erlaubnis zur Aufsuchung bergfreier Bodenschätze zu gewerblichen Zwecken, http://www.lbgr.brandenburg.de/media_fast/4055/Antrag%200_Aufsuchung%20bergfreier%20Bodensch%C3%A4tze_Bkh_20090306.15564291.pdf, 12 pp., last access: 18 December 2014, 2009.

Vattenfall: Hauptbetriebsplan – Aufsuchungsarbeiten in Bezug auf den bergfreien Bodenschatz Sole im Erlaubnisfeld Birkholz-Beeskow, 28 pp., http://www.lbgr.brandenburg.de/media_fast/4055/Bkh_HBP_Finale.pdf, last access: 18 December 2014, 2010.

Vilarrasa, V. and Carrera, J.: Geologic carbon storage is unlikely to trigger large earthquakes and reactivate faults through which CO_2 could leak. Proc. Nat. Acad. Sci. USA, 112 (19), 5938-5943, doi:10.1073/pnas.1413284112, 2015.

Walter, L., Binning, P.J., Oladyshkin, S., Flemisch, B. and Class, H.: Brine migration resulting from CO_2 injection into saline aquifers – An approach to risk estimation including various levels of uncertainty, Int. J. Greenh. Gas Con., 9, 495-506, doi:10.1016/j.ijggc.2012.05.004, 2012.

Wibberley, C. A. J., Yielding, G. and Toro, G.: Recent advances in the understanding of fault zone internal structure: a review. In: Wibberley, C.A.J., Kurz, W., Imber, J., Holdsworth, R.E., Collettini, C. (Eds.), The Internal Structure of Fault Zones: Implications for Mechanical and Fluid-Flow Properties, Geological Society of London, 5-33, doi:10.1144/SP299.2, 2008.

Yamamoto, H., Zhang, K., Karasakib, K., Marui, A., Hitoshi Uehara, H. and Nishikawa, N.: Numerical investigation concerning the impact of CO_2 geologic storage on regional groundwater flow, Int. J. Greenh. Gas Con., 3 (5), 586-599, doi:10.1016/j.ijggc.2009.04.007, 2009.

Zeidouni, M.: Analytical model of leakage through fault to overlying formations, Water Resour. Res., 48, W00N02, 1-17, doi:10.1029/2012WR012582, 2012.

Zhang, K., Wu, Y.S. and Pruess, K.: User's Guide for TOUGH2-MP – A Massively Parallel Version of the TOUGH2 Code, Earth Sciences Division, Lawrence Berkeley National Laboratory, Berkeley, 108 pp., 2008.

Zhou, Q., Birkholzer, J., Mehnert, E., Lin, Y. and Zhang, K.: Modelling Basin- and Plume-Scale Processes of CO_2 Storage for Full-Scale Deployment, Ground Water, 48 (4), 494-514, doi:10.1111/j.1745-6584.2009.00657.x, 2010.

1 Table 1. Summary of numerical simulations of brine migration resulting from CO_2 injection

Authors	Study area and model extend	Reservoir boundaries	Simulator	Injection and duration	Injected fluid	Objectives	Results
Birkholzer et al., 2009	• synthetic • 125 000 km² (radial symmetric)	open	TOUGH2/ ECO2N	1.52 Mt yr^{-1} over 30 years	CO_2	Pressure build-up and brine migration in the reservoir and through low permeable caprocks	• Considerable pressure build-up in a distance of > 100 km from injection zone • Vertical brine migration through a sequence of seals extremely unlikely
Birkholzer et al., 2011	• synthetic • 12 km² (radial symmetric)	closed	TOUGH2/ EOS7	Simulated by pressure build-up	-	Brine migration up a leaking wellbore	• Continuous flow only occurs if pressure perturbation in the reservoir is large enough to overcome the increased weight of the fluid column
Nicot, 2008	• Gulf Coast, USA • 80 000 km²	closed	MODLFLOW96	50 Mt yr^{-1} and 250 Mt yr^{-1} over 50 years	Water	Pressure build-up and brine migration in the reservoir and through low permeable caprocks	• Average water table rise is in the same order of magnitude as seasonal and inter-annual variations
Oldenburg and Rinaldi, 2011	• synthetic • 1 km (2D)	closed	TOUGH2/ EOS7	Simulated by pressure build-up	-	Brine displacement in shallower aquifers through a vertical conduit (borehole or fault)	• Depending on brine density and pressure gradient fluid migrates upward until a new static steady-state equilibrium is reached or a sustained flow develops, if the brine is allowed to spread laterally.
Person et al., 2010	• Illinois basin, USA • 3 000 km² - 241 000 km²	closed and open	Analytical single phase and sharp-interface models	80 Mt yr^{-1} over 100 years		Pressure build-up and CO_2/brine migration in the reservoir and through low permeable caprocks	• No significant lateral brine migration due to distributed injection and vertical brine leakage across the confining unit • Pressure propagation (> 0.3 bar) up to a distance of 10-25 km away from the injection wells
Tillner et al., 2013	• North German Basin • 1 764 km²	closed and open	TOUGH2-MP/ ECO2N	1.7 Mt yr^{-1} over 20 years	CO_2	Brine migration through faults dependent on reservoir compartmentalisation and fault permeability	• Degree of pressurization is the driving mechanism for brine migration • Permeability of fault zones does not influence salinization of shallower aquifers significantly
Yamamoto et al., 2009	• Bay of Tokyo, Japan • 4 200 km²	open	TOUGH2-MP/ ECO2N	10 Mt yr^{-1} over 100 years	CO_2	Pressure build-up and brine migration in the reservoir and through low permeable caprocks	• Pressure build-up of a few bars can occur in the shallow confined aquifers over extensive regions

Authors	Study area and model extend	Reservoir boundaries	Simulator	Injection and duration	Injected fluid	Objectives	Results
Zhou et al., 2010	• Illinois basin, USA • 241 000 km²	open	TOUGH2 - ECO2N	100 Mt yr^{-1} over 50 years	CO_2	Pressure build-up and CO_2/brine migration in the reservoir and through low permeable caprocks	• Pressure build-up of 1 bar and 0.1 bar can be expected as far as 150 km and 300 km from the injection area, respectively • pressure increase of 35 bar at injection does not affect caprock integrity
This study	• North German Basin • 10 000 km²	closed and open	TOUGH2-MP/ ECO2N	1.7 Mt yr^{-1} over 20 years	Water	Brine migration through fault zones depending on different geological conditions	• Boundary conditions, fault length and existence of an overlying secondary reservoir affect pressure development in the reservoir and thereby freshwater salinization

Table 2. Vertical grid discretization, depth and hydraulic parameters for the active geological units.

Unit	k (mD)	Φ (%)	thickness (m)	depth (m)	element layers	vertical resolution (m)
Rupelian basal sands	1 000	20	20	-110 to -130	2	10
Muschelkalk Formation	200	20	140	-1 025 to -1 165	7	19.9
Detfurth Formation	400	17	23	-1 425 to -1 448	2	11.5
Faults	700	18.5			50	19.9

Table 3. Overview about all calculated scenarios assuming a fault permeability of 700 mD. Maximum pressure increase at the base of Fault 1 and displacement depths in Fault 1 are observed at the central part of the fault.

Scenario	Fault length (km)	Effective damage zone volume (m^3)	Δp at base of Fault 1 (bar) [a]	Maximum displacement depth in Fault 1 (m) [ab]	Rupelian basal sand			Duration of mass flow (yrs) [d]
					Relative salt mass change (kg)[a]	Salinization area (m^2) [ac]	Average salt mass in salinization area (kg m^{-2}) [a]	
$F_1^{2km}\ B_C$	2	1.8 x 10^8	19.0	131.7	6.17 x 10^9	1.98 x 10^7	311.6	330
$F_1^{2km}\ B_O$			12.4	105.4	4.86 x 10^9	1.64 x 10^7	296.3	31
$F_1^{2km}\ B_C\ SR_{200mD}$			9.0	69.5	2.93 x 10^9	1.41 x 10^7	207.8	1050
$F_1^{2km}\ B_O\ SR_{200mD}$			6.1	56.3	2.34 x 10^9	1.24 x 10^7	188.7	31
$F_1^{2km}\ B_C^*$			18.9	131.7	5.80 x 10^8	2.11 x 10^7	27.5	275
$F_1^{60km}\ B_C$	60	4.9 x 10^9	12.1	29.8	1.08 x 10^{10}	7.65 x 10^7	141.2	115
$F_1^{60km}\ B_O$			9.7	28.4	8.45 x 10^9	6.73 x 10^7	125.6	31
$F_1^{60km}\ B_C\ SR_{200mD}$			6.8	17.0	5.36 x 10^9	5.89 x 10^7	91.0	390
$F_1^{60km}\ B_O\ SR_{200mD}$			5.3	16.3	4.16 x 10^9	5.09 x 10^7	81.7	40
$F_{1\text{-}4}^{193km}\ B_C$	193	1.6 x 10^{10}	11.0	28.6	1.23 x 10^{10}	1.46 x 10^8	84.2	66
$F_{1\text{-}4}^{193km}\ B_O$			9.6	28.0	9.46 x 10^9	1.21 x 10^8	78.2	42
$F_{1\text{-}4}^{193km}\ B_C\ SR_{200mD}$			6.4	16.5	6.64 x 10^9	1.14 x 10^8	58.2	225
$F_{1\text{-}4}^{193km}\ B_O\ SR_{200mD}$			5.3	16.1	4.59 x 10^9	9.01 x 10^7	50.9	45
$F_{1\text{-}4}^{193km}\ B_O\ SR_{2000mD}$			1.2	4.0	1.06 x 10^9	6.03 x 10^7	17.6	23
$F_1^{2km}\ B_C^*$			10.9	28.6	1.67 x 10^8	1.66 x 10^7	10.1	66

[a] *t = 20 years*

[b] *counting from the base of the Rupelian basal sand*

[c] *salt concentration > 0.5 g kg^{-1} solution*

[d] *mass flow into the Rupelian basal sand > 0.1 kg s^{-1}*

[*] *Salinity gradient of 0.23 g kg^{-1} solution per meter*

Table 4. Overview about six scenarios assuming a sharp salt-/freshwater interface below the base of the Rupelian basal sand and a fault permeability of 10 mD, 200 mD and 700 mD, respectively. Maximum pressure increase at the base of Fault 1 and displacement depths in Fault 1 are again observed at the central part of the fault.

Scenario	**Fault permeability (mD)**	**Δp at base of Fault 1 (bar)** [b]	**Maximum displacement depth in fault (m)** [ab]	**Rupelian basal sand**			**Duration of mass flow (yrs)** [d]
				Relative salt mass change (kg) [ab]	**Salinization area (m^2)** [ac]	**Average salt mass in salinization area ($kg\ m^{-2}$)** [a]	
	10	12.1	9.1	5.15×10^9	1.02×10^8	50.6	310
$F_{1\text{-}4}^{193km}\ B_C\ SR_{200mD}$	200	7.0	17.9	6.50×10^9	1.11×10^8	58.6	270
	700	6.4	16.5	6.64×10^9	1.14×10^8	58.2	225
	10	10.9	8.7	3.66×10^9	8.91×10^7	41.1	46
$F_{1\text{-}4}^{193km}\ B_O\ SR_{200mD}$	200	5.9	17.6	4.52×10^9	8.58×10^7	52.7	45
	700	5.3	16.1	4.59×10^9	9.01×10^7	50.9	45

[a] *t = 20 years*

[b] *counting from the base of the Rupelian basal sand*

[c] *salt concentration > 0.5 g kg^{-1} solution*

[d] *mass flow into the Rupelian basal sand > 0.1 kg s^{-1}*

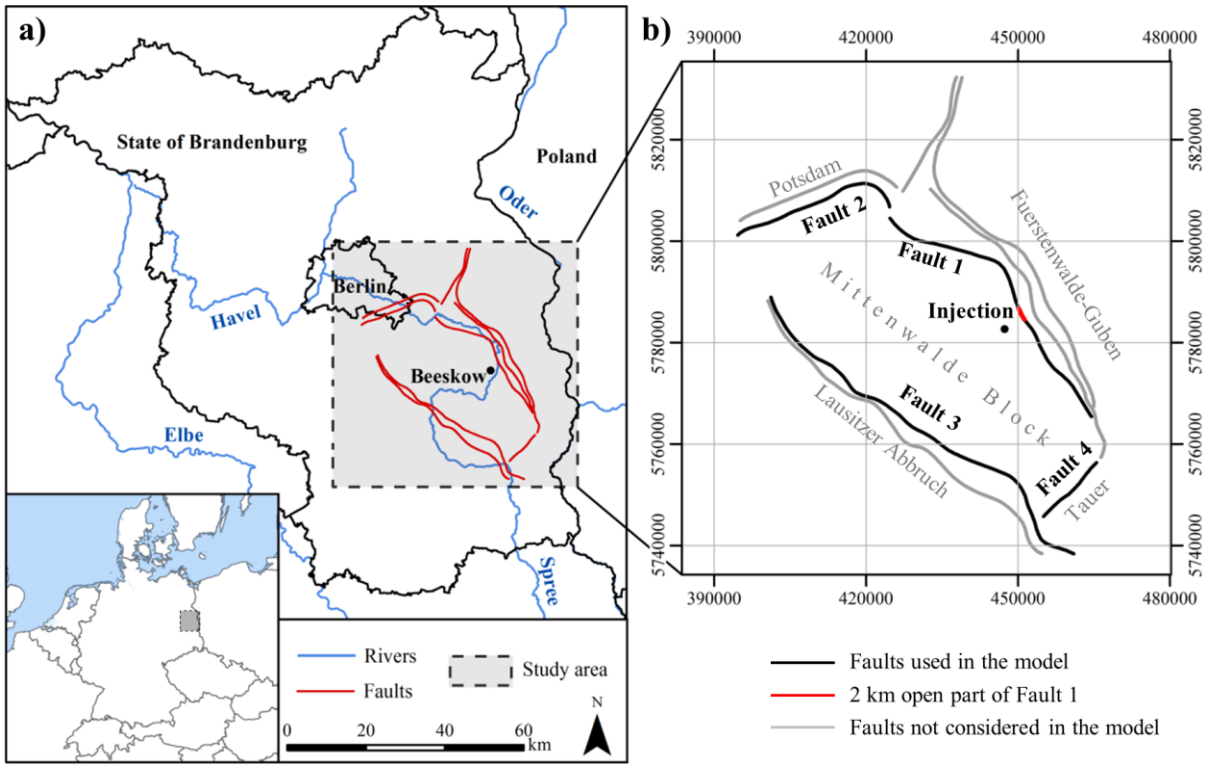

Figure 1. (a) Dashed rectangle indicates the location of the study area in the State of Brandenburg (Germany), while red lines illustrate the present fault systems. (b) Only the inner faults (black lines), facing to the injection well, were implemented to represent the entire fault zone. Axes show UTM-coordinates (WGS84/UTM zone 33N). Rivers and the outline of the states of Brandenburg and Berlin were derived from Tillner et al. (2013).

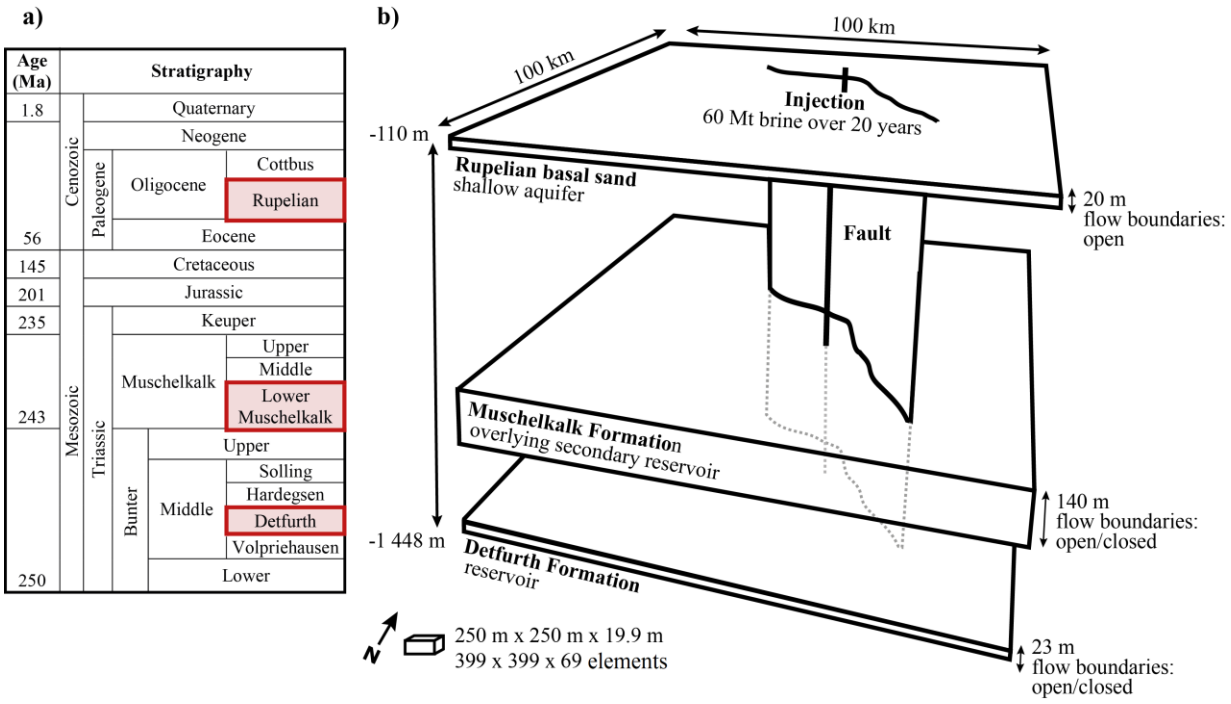

1

2 Figure 2. (a) Stratigraphy of the study area with the active model layers highlighted in red.
3 (b) The geological 3D model with simplified topography comprises up to three layers.

4

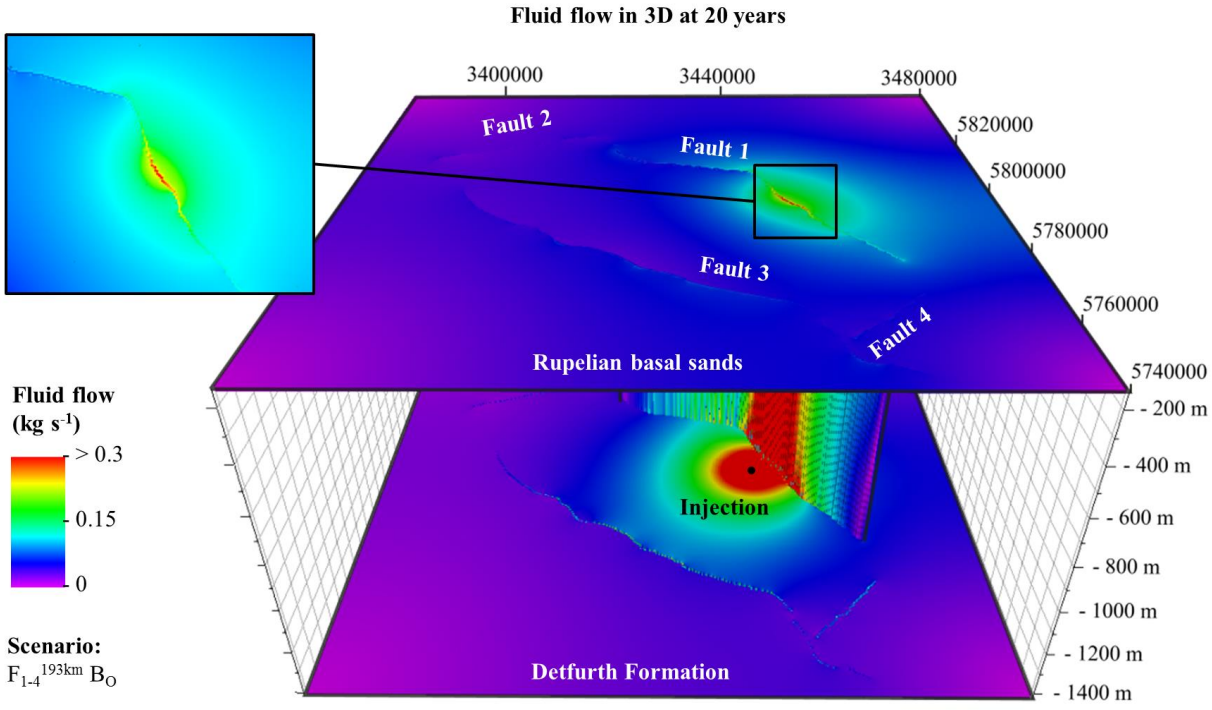

Figure 3. In all scenarios, brine is displaced radially within the reservoir and predominantly into parts of the faults lying closer to the injection well as illustrated for Scenario $F_{1\text{-}4}^{193km}\ B_O$.

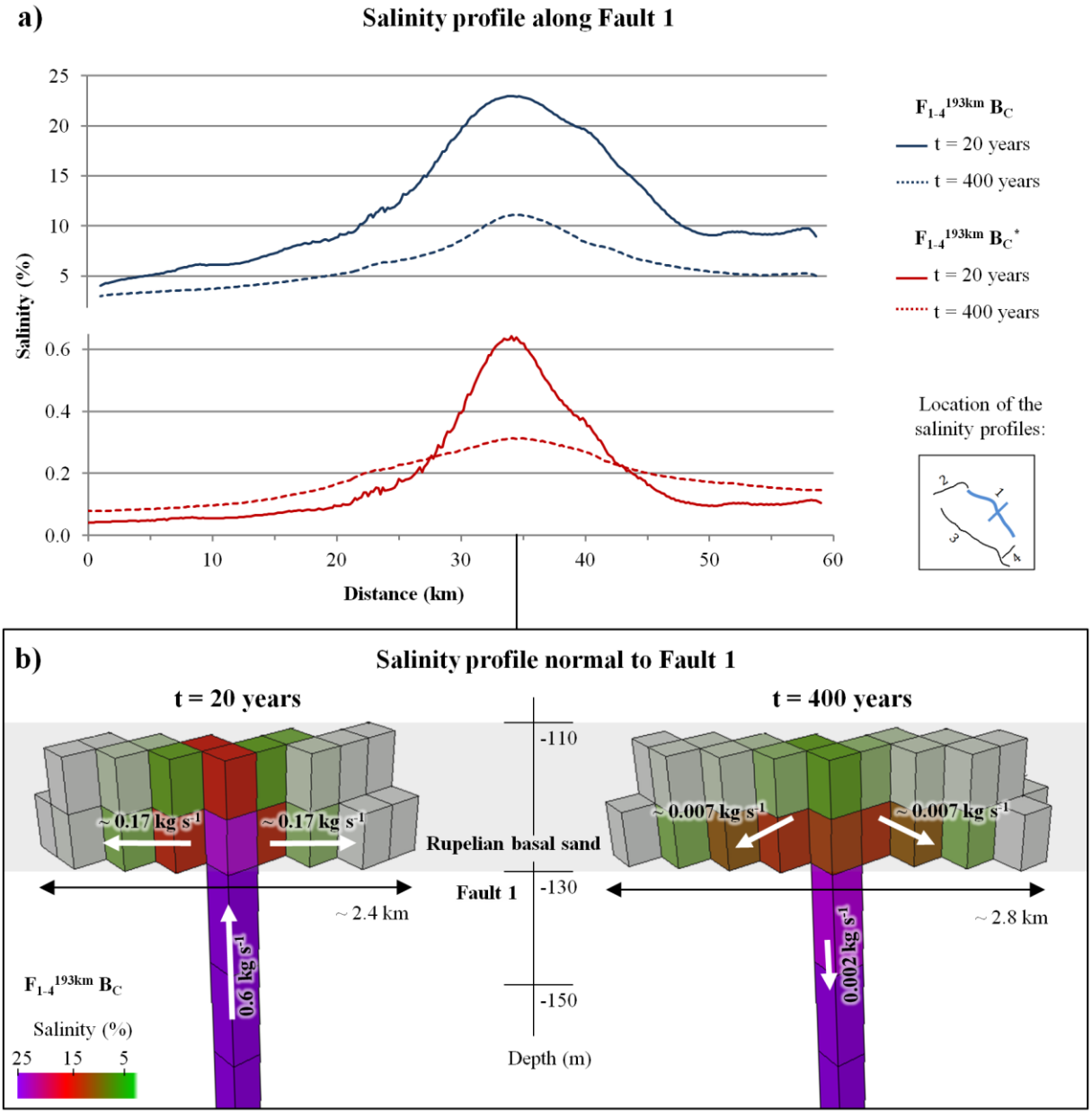

Figure 4. (a) Profile along Fault 1 shows highest salinities in the central part of the fault near to the injection well. Maximum salinities are significantly lower, if a salinity gradient is assumed (solid red line; Scenario $F_{1\text{-}4}^{193km}\ B_C^{*}$). A decrease in salinization due to a downward flow is observed for the time after the injection period and under the assumption of a sharp salt-/freshwater interface (dashed blue line; Scenario $F_{1\text{-}4}^{193km}\ B_C$). (b) Cross section normal to Fault 1 illustrates the propagation of the saltwater plume (salinities > 0.05 %), while higher salinities can be observed within the lower element layer. White arrows illustrate schematically the direction of the fluid flow at 20 years and 400 years.

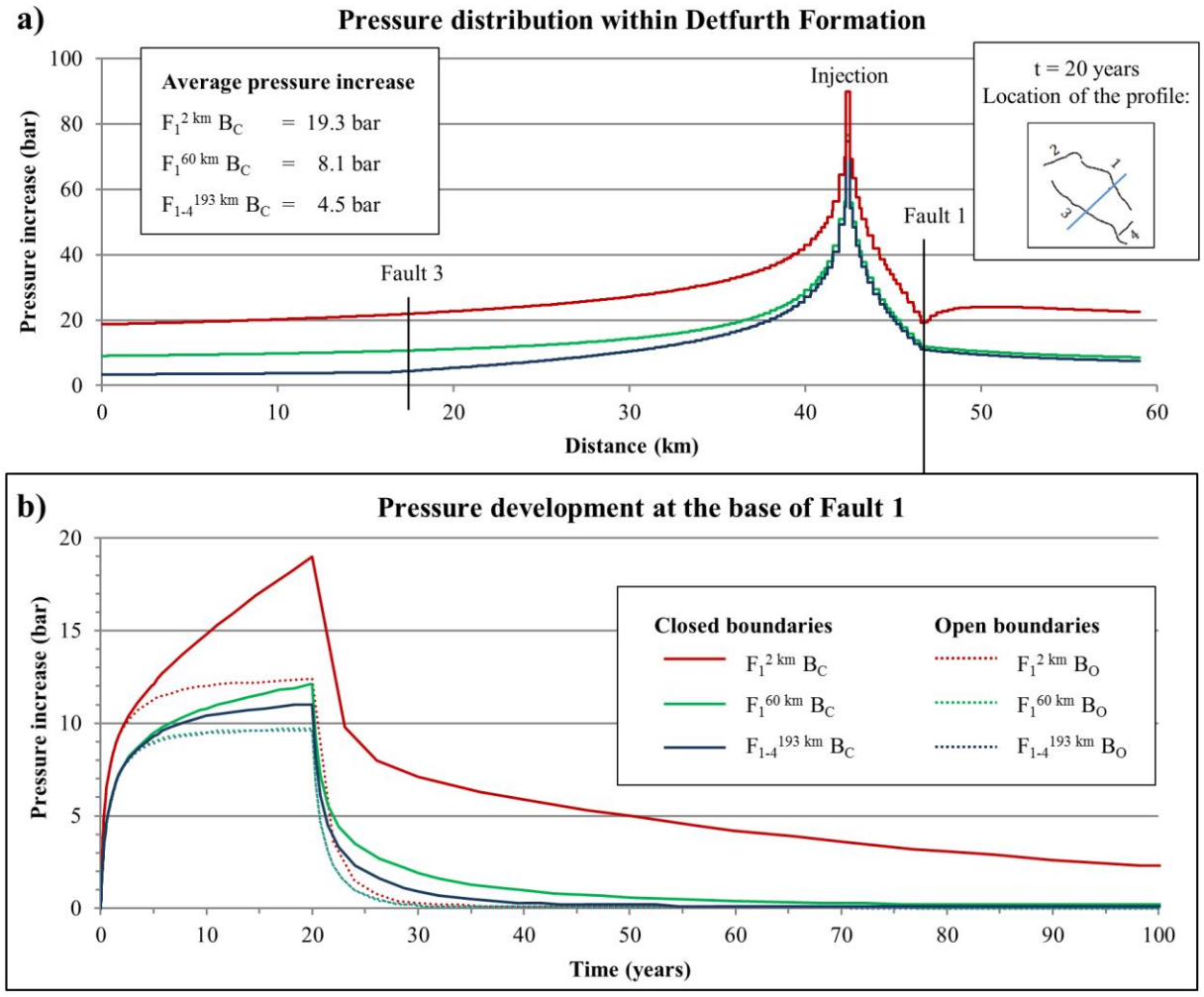

Figure 5. (a) Distribution of the pressure increase within the Detfurth Formation along the highlighted cross section significantly varies depending on the open fault length. Highest pressurization is observed for a short fault (F_1^{2km} B_C). (b) Pressure development at the base of Fault 1 indicates a substantially faster pressure reduction for greater fault lengths.

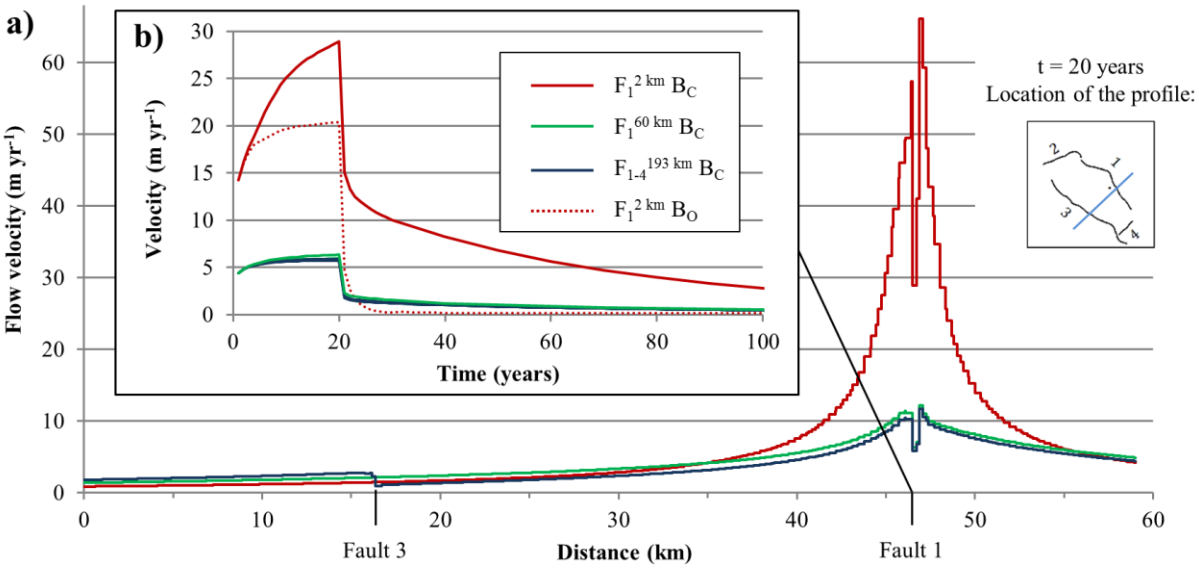

Figure 6. (a) Velocity profile within the lower element layer of the Rupelian basal sand shows highest flow velocities out of Fault 1 at the end of injection period. (b) Flow velocities out of Fault 1 increase until the end of the injection period (20 years) and decrease afterwards depending on pressure reduction of the respective scenarios.

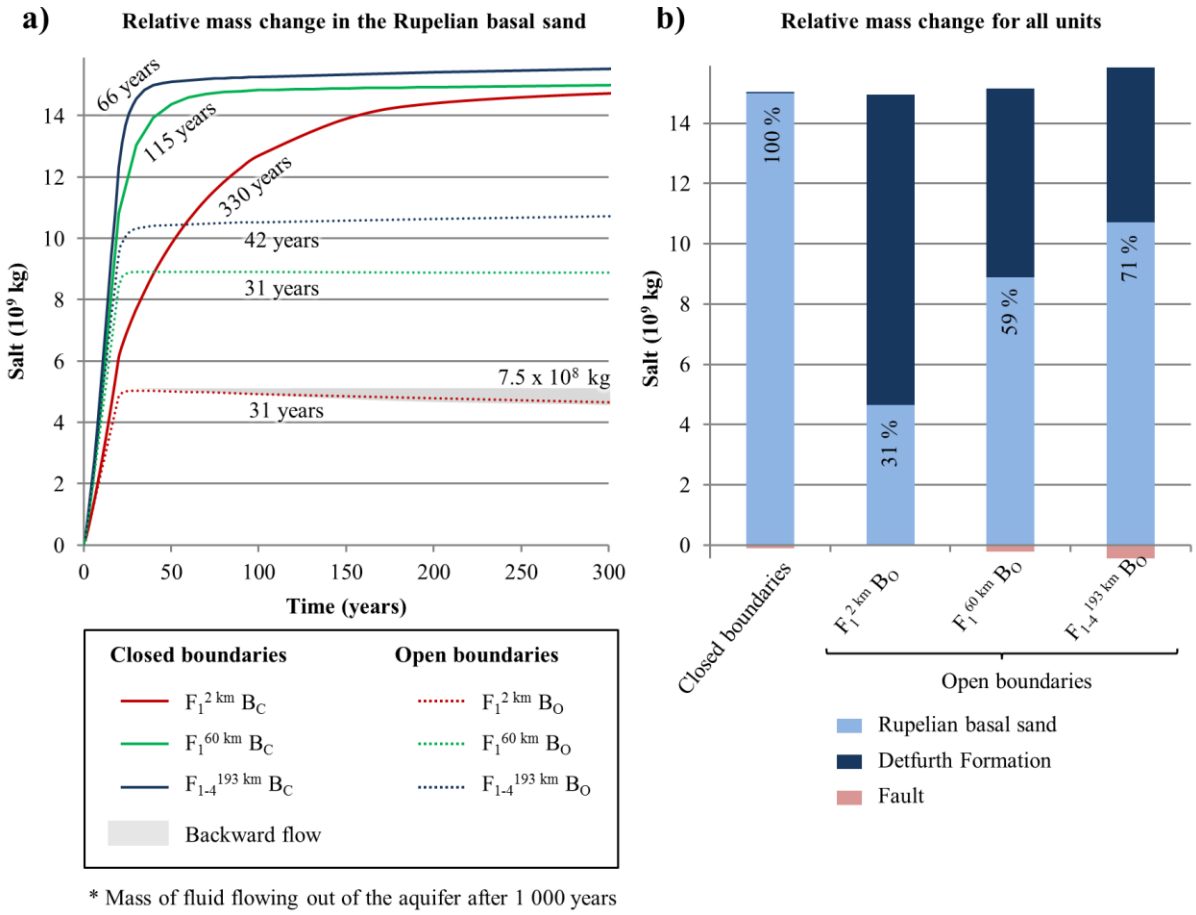

Figure 7. (a) Relative salt mass change in the Rupelian basal sand shows that the mass of salt displaced into the shallow aquifer corresponds to the overall injected fluid mass, if reservoir boundaries are closed. As indicated by the duration of mass flow (black numbers), only a temporal effect on fluid migration occurs. (b) Relative mass change for all lithological units after 20 years illustrates a considerably reduced salinization of the Rupelian basal sand for open reservoir boundaries.

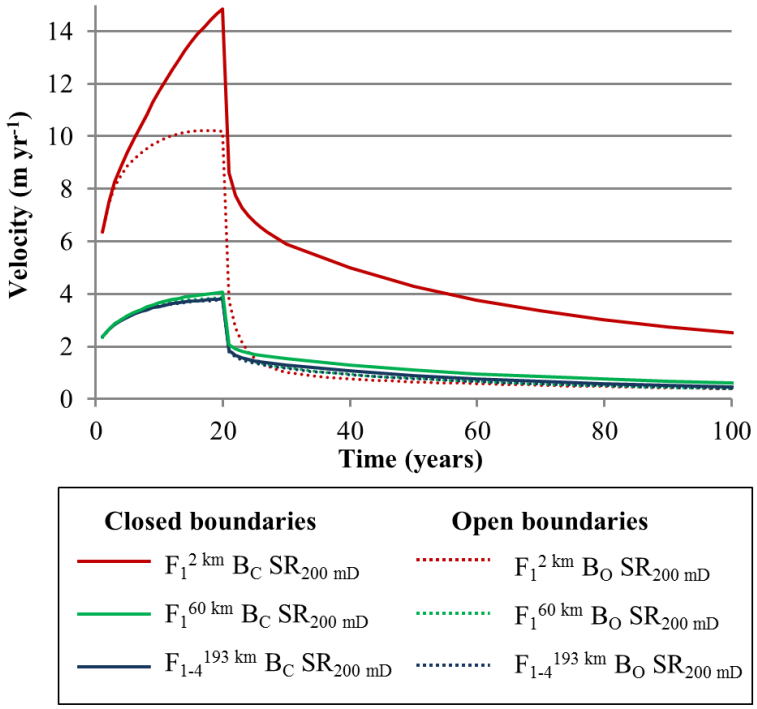

Figure 8. The temporal evolution of the flow velocities out of Fault 1 show a substantial reduction due to lower reservoir pressures for the scenarios considering a secondary overlying reservoir as well as open boundaries.

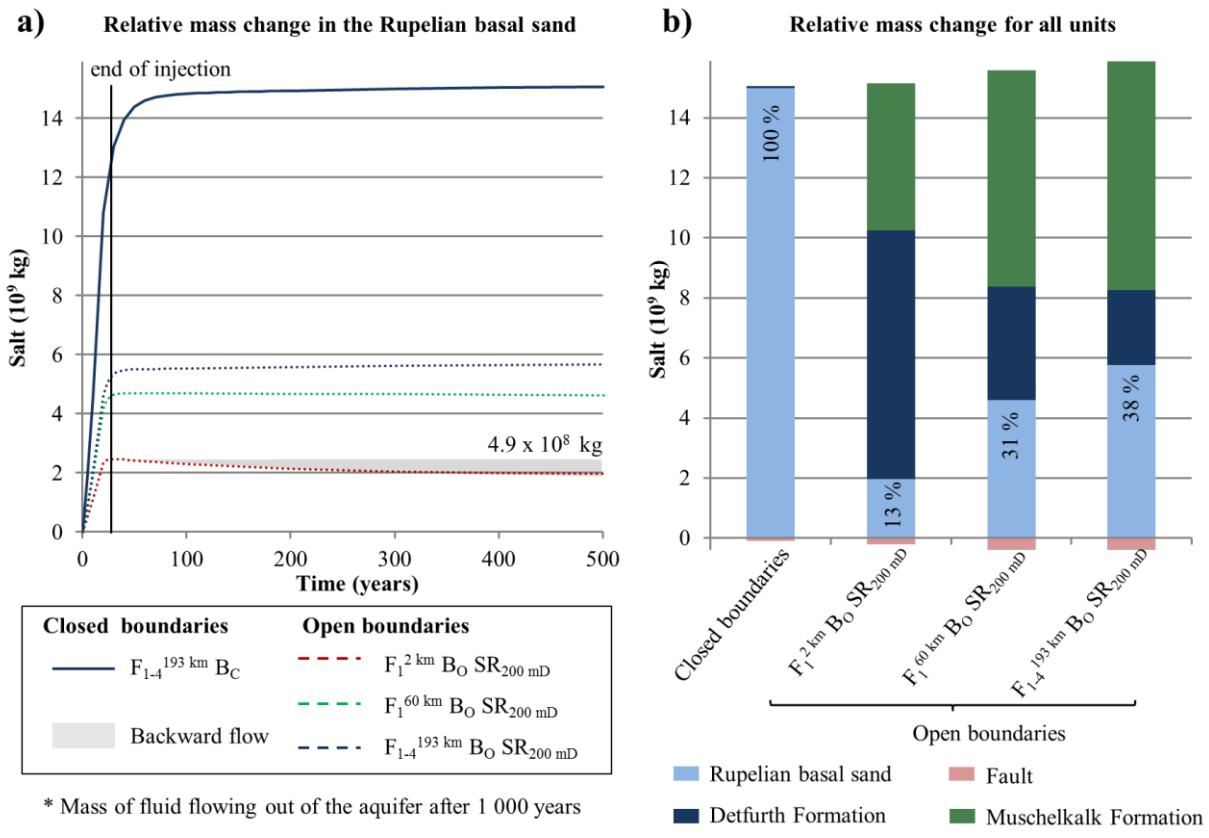

Figure 9. (a) Temporal evolution of the relative mass change of the Rupelian basal sand shows a lower duration of mass flow for open reservoir boundary conditions. Further, a slight backward flow out of the aquifer can be observed if the hydraulically conductive fault length is small. (b) Relative mass change for lithological units at 1 000 years (considering the backflow) illustrates, that salinization in the shallow aquifer is substantially reduced, if reservoir boundaries are open, and further an overlying secondary reservoir exists.

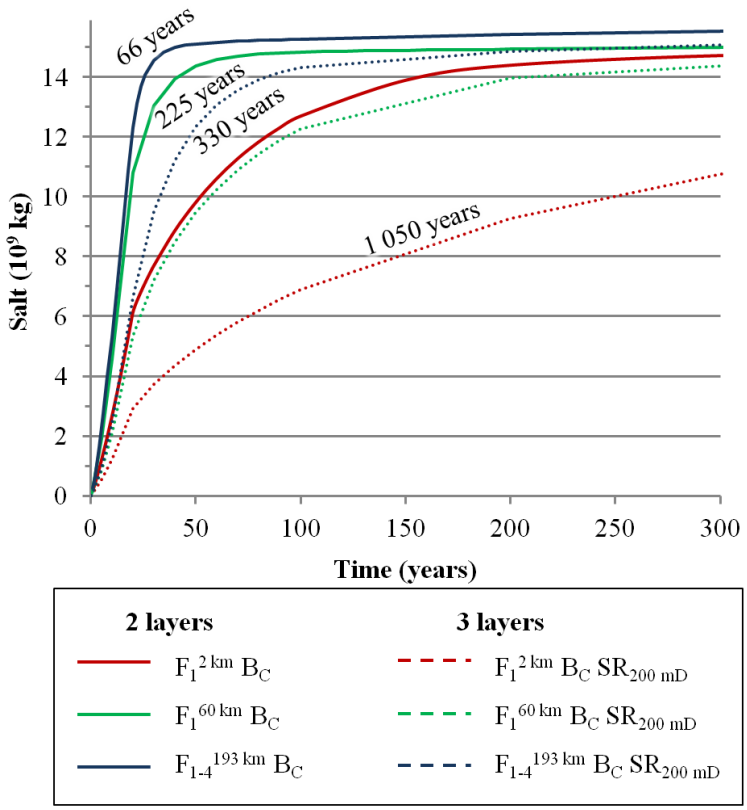

Figure 10. Relative salt mass change of the Rupelian basal sand illustrates the retardation in fluid flow (black numbers) in case of closed reservoir boundaries and due to the presence of an overlying reservoir. The salt mass that is displaced into the shallow aquifer is almost identical, when pressure comes to equilibrium.

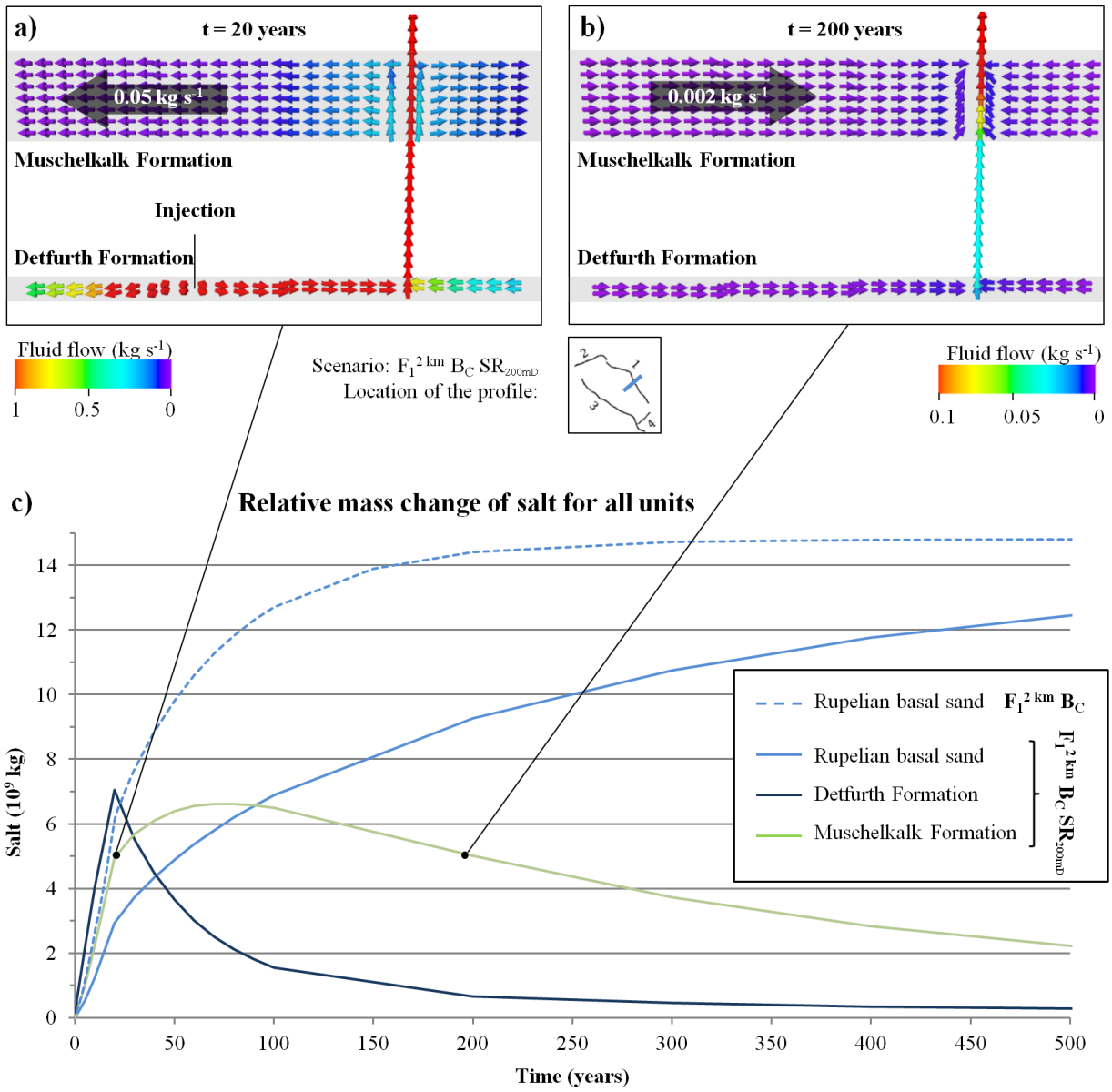

Figure 11. (a) Cross profile normal to Fault 1 shows, that during the injection period the displaced fluid spreads within the Detfurth and the Muschelkalk. (b) Afterwards, the overpressure in both reservoirs is successively reduced and brine is transported out of the respective reservoir and into the Rupelian basal sand. (c) Temporal evolution of the relative salt mass change shows the resulting retardation in fluid flow into the Rupelian basal sand for Scenario F_1^{2km} B_C SR_{200mD}.

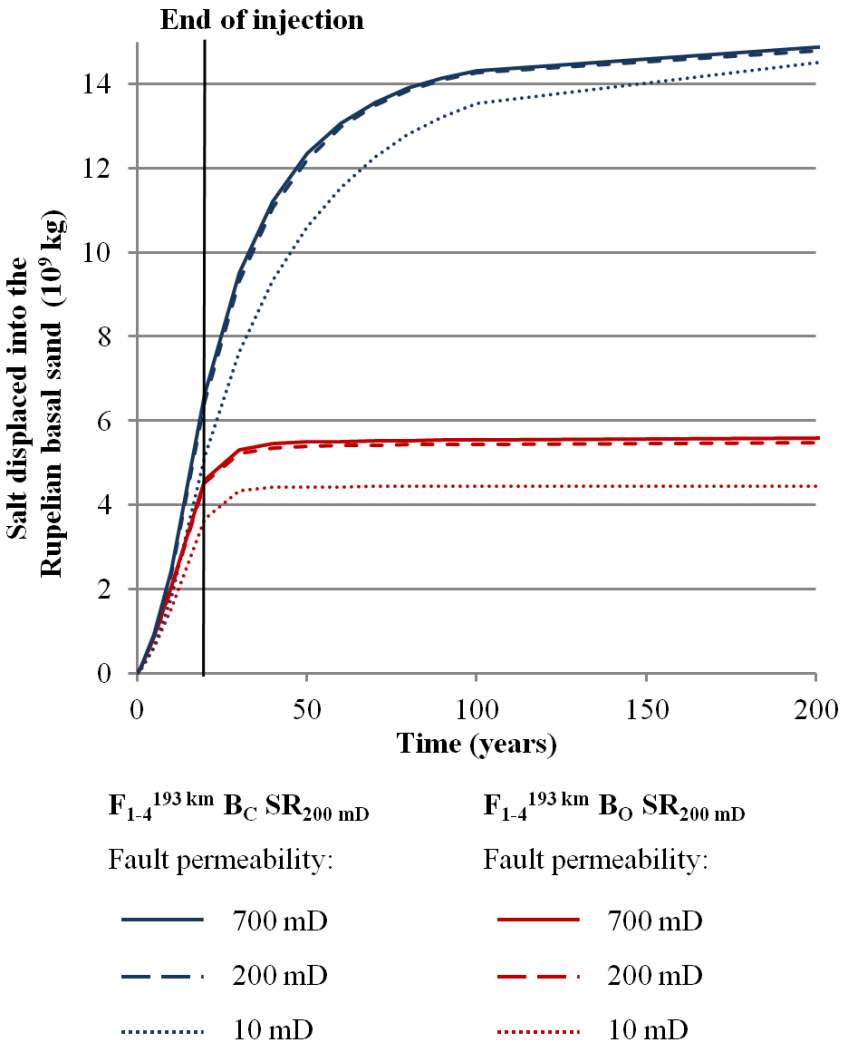

Figure 12. Salt mass displaced into the Rupelian basal sand assuming four open faults with varying permeability, a secondary overlying reservoir and open (red) or closed (blue) reservoir boundaries. The salt mass displaced into the Rupelian basal sand at the time of the injection stop and thereafter is almost identical for a fault permeability higher (solid lines) or equal (dashed lines) to the permeability of the secondary reservoir. If fault permeability is lower than that of the secondary reservoir (dotted lines), less salt is displaced into the shallow aquifer. Closed reservoir boundaries and low-permeable faults lead to retardation in mass flow (blue dotted line).

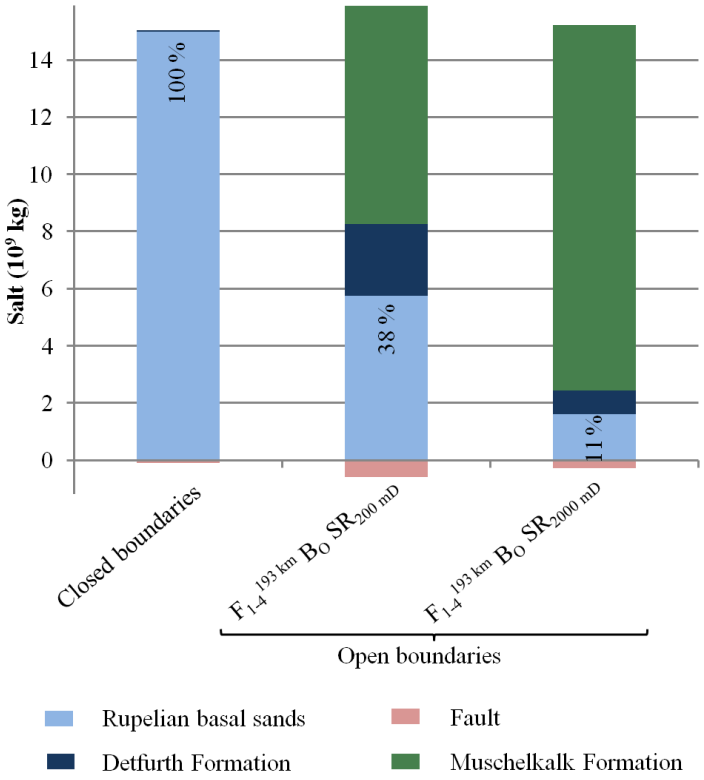

Figure 13. Relative mass change for all lithological units after 1 000 years illustrates that if permeability of the fault is lower than of the Muschelkalk Formation ($F_{1\text{-}4}^{193km}\,B_O\,SR_{2000mD}$) brine is preferentially displaced into the overlying secondary reservoir. Consequently, freshwater salinization in the shallow aquifer is lowest compared to all other scenarios with a sharp salt-/freshwater interface.

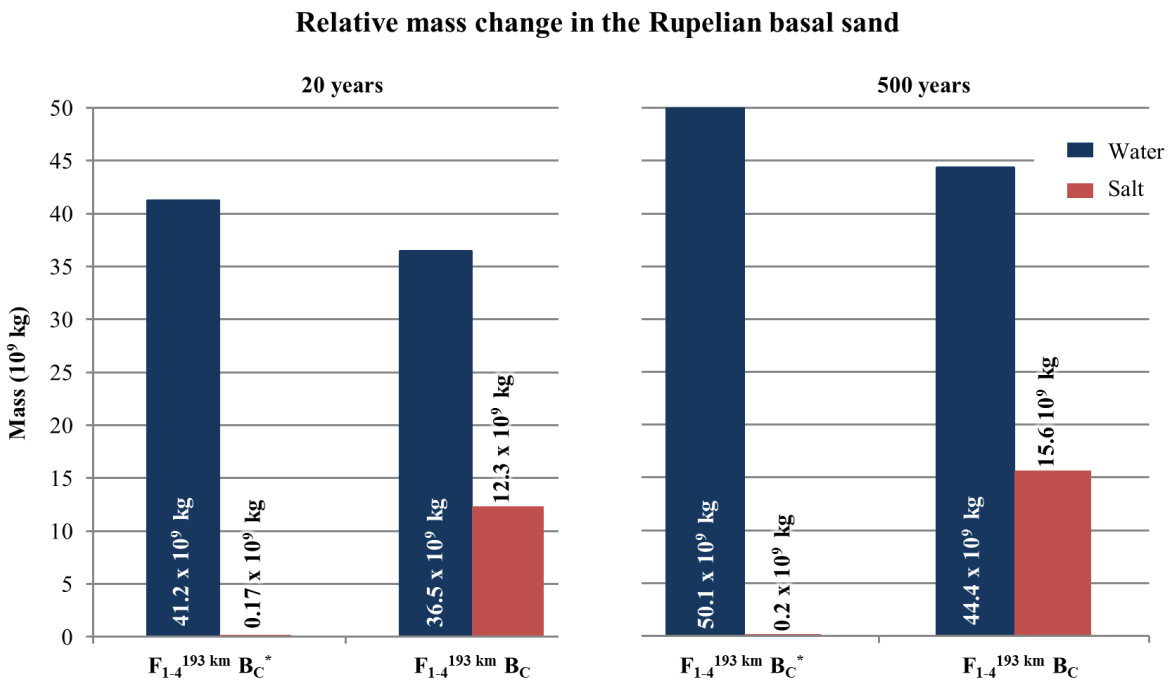

Figure 14. Relative mass change in the Rupelian basal sand after 20 years and 500 years for Scenario $F_{1\text{-}4}^{193km}$ B_C with a sharp salt-/freshwater boundary below the base of the Rupelian and Scenario $F_{1\text{-}4}^{193km}$ B_C^* with salinity increasing with depth by 0.23 g kg^{-1} solution per meter up to a maximum of 250 g kg^{-1} at a depth of 1 070 m.